Extended Multiplexing of Tandem Mass Tags (TMT) Labeling Reveals Age and High Fat Diet Specific Proteome Changes in Mouse Epididymal Adipose Tissue*[S]

Deanna L. Plubell‡, Phillip A. Wilmarth§, Yuqi Zhao¶, Alexandra M. Fenton‡, Jessica Minnier‡, Ashok P. Reddy§, John Klimek§, Xia Yang¶, Larry L. David§, and Nathalie Pamir‡‖

The lack of high-throughput methods to analyze the adipose tissue protein composition limits our understanding of the protein networks responsible for age and diet related metabolic response. We have developed an approach using multiple-dimension liquid chromatography tandem mass spectrometry and extended multiplexing (24 biological samples) with tandem mass tags (TMT) labeling to analyze proteomes of epididymal adipose tissues isolated from mice fed either low or high fat diet for a short or a long-term, and from mice that aged on low *versus* high fat diets. The peripheral metabolic health (as measured by body weight, adiposity, plasma fasting glucose, insulin, triglycerides, total cholesterol levels, and glucose and insulin tolerance tests) deteriorated with diet and advancing age, with long-term high fat diet exposure being the worst. In response to short-term high fat diet, 43 proteins representing lipid metabolism (*e.g.* AACS, ACOX1, ACLY) and red-ox pathways (*e.g.* CPD2, CYP2E, SOD3) were significantly altered (FDR < 10%). Long-term high fat diet significantly altered 55 proteins associated with immune response (*e.g.* IGTB2, IFIT3, LGALS1) and rennin angiotensin system (*e.g.* ENPEP, CMA1, CPA3, ANPEP). Age-related changes on low fat diet significantly altered only 18 proteins representing mainly urea cycle (*e.g.* OTC, ARG1, CPS1), and amino acid biosynthesis (*e.g.* GMT, AKR1C6). Surprisingly, high fat diet driven age-related changes culminated with alterations in 155 proteins involving primarily the urea cycle (*e.g.* ARG1, CPS1), immune response/complement activation (*e.g.* C3, C4b, C8, C9, CFB, CFH, FGA), extracellular remodeling (*e.g.* EFEMP1, FBN1, FBN2, LTBP4, FERMT2, ECM1, EMILIN2, ITIH3) and apoptosis (*e.g.* YAP1, HIP1, NDRG1, PRKCD, MUL1) pathways. Using our adipose tissue tailored approach we have identified both age-related and high fat diet specific proteomic signatures highlighting a pronounced involvement of arginine metabolism in response to advancing age, and branched chain amino acid metabolism in early response to high fat feeding. Data are available via ProteomeXchange with identifier PXD005953. *Molecular & Cellular Proteomics 16: 10.1074/mcp.M116.065524, 873–890, 2017.*

Obesity is a worldwide epidemic associated with increased incidence of metabolic complications such as type 2 diabetes, hypertension, dyslipidemia, and atherosclerosis. Intra-abdominal adipose tissue is a multifunctional endocrine organ that participates in whole body energy metabolism. Because of its anatomical location, intrinsic properties, and capacity to store and release energy through lipogenesis and lipolysis, it is a primary target of detrimental high fat diets. The obesity-related biological and metabolic changes within abdominal white adipose tissue could elucidate its role in the etiology of obesity related metabolic complications.

The rapid spread of obesity and overweight has prompted efforts to understand the biological and metabolic dynamics of white adipose tissue in response to western living. Much progress has been made in defining the transcriptional networks controlling the terminal differentiation of preadipocytes into mature adipocytes or controlling the whole tissue response to high fat diet (1). However, white adipose tissue protein changes in response to duration of high fat diet and to maturation on either low or high fat diet are still not well understood.

Previous large-scale approaches to evaluate tissue response have been largely limited to gene expression analyses using microarrays or RNA sequencing (2–4). In recent years,

From the ‡Department of Medicine, Knight Cardiovascular Institute, Oregon Health & Sciences University, Portland, Oregon; §Proteomics Shared Resources, Oregon Health & Sciences University, Portland, Oregon; ¶Department of Integrative Biology and Physiology, University of California, Los Angeles, California

Received November 15, 2016, and in revised form, February 28, 2017

Published, MCP Papers in Press, March 21, 2017, DOI 10.1074/mcp.M116.065524

Author contributions: A.P.R., L.L.D., and N.P. designed research; D.L.P., A.M.F., and N.P. performed research; X.Y., L.L.D., and N.P. contributed new reagents or analytic tools; D.L.P., P.A.W., Y.Z., J.M., J.K., and N.P. analyzed data; D.L.P., P.A.W., X.Y., L.L.D., and N.P. wrote the paper.

with advances in proteomic technologies, high-resolution and high-throughput mass spectrometry is routinely used to identify and quantify proteomes of different tissues or cells for target identification (5–7). However, few studies have focused on the proteomic changes of the whole white adipose tissue in response to metabolic changes (8–11). Meierhofer *et al.* pooled the mouse white adipose tissue samples of the same experimental group and analyzed it in duplicate using a mouse stable isotope labeled amino acids in culture (SILAC) sample as a normalization reference (8). This approach, although quantitative, suffers from problems associated with sample pooling in omic studies (12). Two reports in rats investigated changes in white adipose tissue in response to high fat diet or caloric restriction. Using two-dimensional gel electrophoresis (2DE) and MALDI-TOF-MS, Okita and colleagues performed a study to compare the expression of proteins between caloric restriction and control groups in white adipose tissue (WAT) and brown adipose tissue (BAT) of rats. The total number of proteins identified was ~1500, among which only 7 were differentially regulated proteins in WAT in response to caloric restriction (13). With the same approach, Joo and colleagues identified 70 differentially expressed proteins in WAT *versus* BAT. Most of the variations were thermogenic and lipogenic enzymes in adipose tissues of obese prone rats (9). A recent report from Gomez-Serrano *et al.* using 4-plex isobaric labeling and LC-MS to study human visceral adipose depot described similar findings as ours (11); however, their study was limited to single replicates of pooled samples. To summarize, the small volume and high lipid content of the starting material, the numbers of biological replicates, and the difficulties in protein quantification have limited profiling of the global protein changes in adipose tissue. Moreover, the cellular concentrations of proteins have been proven to weakly correlate with the abundances of their corresponding mRNAs (Pearson correlation coefficient r = 0.2~0.5) (14–16), which implies that less than half of the variation in protein concentration can be explained by knowing mRNA abundances.

We have developed a novel approach that uses tandem mass tags (TMT)[1] (17) in combination with in line two-dimensional liquid chromatography tandem mass spectrometry (2D LC-MS/MS) to overcome these limitations. Our goals were: (1) to provide a simple, reproducible, and detailed method for proteome analysis of adipose tissue, (2) to identify proteome changes in response to short- *versus* long-term high fat diet, and (3) to identify aging-related proteome changes while exposed to low *versus* high fat diet.

Through three-dimensional integration of proteome profiles, metabolic profiles, and gene regulatory networks, we have identified unique sets of proteins and gene networks that characterize the changes within adipose tissue in response to short- *versus* long-term high fat feeding. Short-term high fat feeding was associated with mitochondria related metabolic changes and lipid metabolism, whereas long-term feeding led to extracellular matrix remodeling and activation of the immune system. Mice that grew older either on low or high fat diet shared aging-related responses, such as activation of urea cycle and changes in methionine and sulfur metabolism, whereas extracellular remodeling and immune activation was only captured for mice that grew older on high fat diet, thus indicating an interaction between advancing age and diet

EXPERIMENTAL PROCEDURES

Experimental design and statistical rationale—For metabolic experiments, we have used n = 8–13 mice per group. For mass spectrometry experiments we have used a subgroup (of the metabolic experiments) of n = 5 mice (biological replicates) per metabolic condition, as described in Fig. 1. Each TMT set (3 total) included 2 pooled control samples for across TMT-plex normalizations (details below). The samples were randomized using an Excel function. The statistical tests used for each experiment are described within each section.

Materials—Triethylammonium bicarbonate (TEAB), tris(2-carboxyethyl)phosphine (TCEP), Tandem Mass Tag 10-plex isobaric reagents, and organic solvents were from Thermo Fisher Scientific (Rockford, IL). Sequencing grade LysC/trypsin was from Promega (Madison, WI). Unless otherwise noted all other chemicals were from Sigma-Aldrich (St. Louis, MO).

Mice—All studies were approved by the Institutional Animal Care and Use Committee of the University of Washington. C57Bl/6J male mice (Jackson Labs, #000664) were housed (3–5 mice per cage) in a specific pathogen-free barrier facility in a temperature-controlled room (22 °C) with a 12-h light/dark cycle, and given free access to food and water. At 8 weeks of age, the mice were fed either a low-fat (4%) regular chow diet (Wayne Rodent BLOX 8604; Harlan Teklad Laboratory, Madison, WI), or a high-fat (60% calories from fat, Bioserve, Flemington, NJ, #F1850) diet and were analyzed at 16 weeks and 26 weeks of age. Before necropsy, mice were fasted for 4 h in the morning, bled from the retro-orbital sinus into tubes containing 1 mM EDTA, and euthanized by isofluorane inhalation. Whole epididymal adipose depots were collected, weighted, snap frozen in liquid nitrogen, and stored at −80 °C until analysis. For metabolic measurements, we have based the numbers of mice required on previously published research by our group (18, 19)

Insulin and Glucose Tolerance Testing—Insulin and glucose tolerance tests were performed after a 4-h fast. Mice were injected intraperitoneally with human insulin (1.0 U/kg body weight; Eli Lilly, Indianapolis, IN) or glucose (1 mg/g body weight) (20) and blood glucose level was measured at baseline, 15, 30, 60, and 120 min time points.

Adipose Tissue Fractionation—Under sterile conditions, adipose tissue was extracted and separated into stromal vascular cell and adipocyte fractions (21). Minced tissue in digestion buffer (Dulbecco's PBS supplemented by calcium and magnesium, Thermo Scientific) was incubated with 2 mg/ml type I collagenase (Worthington, Lakewood, NJ) for 45 min at 37 °C on an orbital shaker, filtered through 250 μm nylon mesh, and centrifuged at 500 × g for 5 min. The pellet was resuspended in erythrocyte lysis buffer (Cell Signaling, Danvers, MA), incubated at room temperature for 5 min, and then filtered through a 70 μm nylon mesh and washed by centrifugation as above.

Plasma Glucose, Insulin, and Lipid Measurement—At the time of sacrifice, blood was collected after a 4 h fast, and insulin, triglyceride, and cholesterol levels were determined using an ultrasensitive insulin ELISA (Linco, Billerica, MA), L-Type TG M assay (Wako Diagnostics,

[1] The abbreviations used are: TMT, tandem mass tags; LC-MS/MS, liquid chromatography-tandem MS; IRS, internal reference scaling; FDR, false discovery rate.

Richmond, VA), and Amplex Red Cholesterol Assay Kit (Invitrogen, Carlsbad, CA).

Real-time Quantitative RT-PCR—Total RNA samples were isolated from epididymal adipose tissue using the EZNA Total RNA kit II (Omega, Norcross, GA) and quantified by spectrometry. First-strand cDNAs were synthesized from 0.1 to 0.5 mg of total RNA using iScript cDNA synthesis kit (BioRad, Hercules, CA). Primers and probes were purchased from Thermo Fisher; IL12-α (cat: Mm00434165), IL1-β (cat: Mm00434228), RpL32 (cat: Mm02528467), IL-6 (cat: Mm00446191), Tnf-α (cat:Mm00443258). Results were analyzed using the CT method (22).

Adipose Tissue Protein Isolation—One hundred to 300 mg of epididymal adipose tissue from individual mice was homogenized on ice in 1 ml homogenization buffer (150 mM NaCl, 50 mM HEPES pH 8.5, 1× GBiosciences ProteaseArrest) using a polytron tissue homogenizer. Homogenized samples were spun at 10,000 × *g* for 10 min at 4 °C and the top lipid layer removed. Supernatant and pellet were lysed by addition of SDS to a final concentration of 2.5% and sonicated three times at 2 watts for 5 s each with 30 s rests between. Chloroform-methanol precipitation was performed to further eliminate lipids. In brief, four parts methanol, two parts chloroform, and three parts water were added to each sample, mixed, and spun down. The top fraction was removed and the protein layer was washed four times with 100% methanol. Proteins were dried by vacuum centrifugation and stored at −80 °C.

Tryptic Digest—Epididymal adipose protein samples were reconstituted in 50 mM HEPES with brief sonication to aid in protein solubilization, and protein concentration was determined using the Pierce bicinchoninic acid (BCA) protein assay with a BSA standard (Thermo Fisher Scientific, Rockford IL). The following steps were carried out with 100 μg protein of each sample in 0.1% Rapigest (Waters, Milford, MA). Disulfide bonds were reduced with 5 mM tris(2-carboxyethyl) phosphine (TCEP) for 30 min at 37 °C. Cysteines were alkylated with 15 mM iodoacetamide for 30 min at room temperature in the dark. Excess iodoacetamide was quenched with 5 mM DTT for 15 min at room temperature in the dark. Protein was digested with a mixture of LysC and Trypsin (Cat # V5071, Promega, Madison, WI) at a 1:100 w/w protease/protein ratio for 3 h at 37 °C, then at a 1:50 w/w ratio overnight at 37 °C. Digestion was terminated by the addition of trifluoroacetic acid to 0.5%. Particulates were then removed by spinning at 12,000 × *g* for 15 min, and peptides were solid phase extracted using Waters Sep-Pak tC18 cartridges according to manufacturer's instructions, dried down, and stored at −80 °C.

TMT Labeling—Peptides were reconstituted in 100 mM triethylammonium bicarbonate (TEAB) and their concentration determined by the BCA assay described above. A pooled sample for normalization between runs was prepared by combining 6.25 μg of peptide from each individual sample. TMT labeling was carried out on 25 μg of peptides from each individual sample and the pooled sample. Samples were randomly distributed between three 10-plex label sets, along with 2 pooled samples per set. TMT 10-plex labeling reagents (0.8 mg) were each dissolved in 52 μl anhydrous acetonitrile (ACN). Each sample containing 25 μg of peptide in 25 μl volume of TEAB buffer was combined with 12 μl of its respective 10-plex TMT reagent and incubated for 1 h at room temperature. Two μl of each reaction mixture was then mixed, 2 μl of 5% hydroxylamine added, and the combined sample incubated for a further 15 min. The mixture was then dried down, dissolved in 5% formic acid, and 2 μg of peptide analyzed by a single 2 h LC-MS/MS method using an Orbitrap Fusion as described below. This run was performed to normalize the total reporter ion intensity of each multiplexed sample and check labeling efficiency. The remaining samples were quenched by addition of 2 μl of 5% hydroxylamine as above, then combined in a 1:1:1:1:1:1:1:1:1:1 ratio based on total reporter ion intensities determined during the normalization run, and dried down in preparation for 2D-LC-MS/MS analysis.

LC-MS/MS Analysis— TMT (17), isobaric quantitative labeling reagent, allows up to 10 biological samples to be analyzed in a single mass spectrometry experiment. High-resolution instruments with advanced ion collection methods (23) allow highly multiplexed studies where expression changes can be measured with wide dynamic range and excellent accuracy.

Multiplexed TMT-labeled samples were reconstituted in 5% formic acid and separated by two-dimensional reverse-phase liquid chromatography using a Dionex NCS-3500RS UltiMate RSLCnano UPLC system. A 20 μl sample (40 μg) was injected onto a NanoEase 5 μm XBridge BEH130 C18 300 μm x 50 mm column (Waters) at 3 μl/min in a mobile phase containing 10 mM ammonium formate (pH 9). Peptides were eluted by sequential injection of 20 μl volumes of 14, 20, 22, 24, 26, 28, 30, 40, and 90% ACN in 10 mM ammonium formate (pH 9) at 3 μl/min flow rate. Eluted peptides were diluted with mobile phase containing 0.1% formic acid at 24 μl/min flow rate and delivered to an Acclaim PepMap 100 μm x 2 cm NanoViper C18, 5 μm trap on a switching valve. After 10 min of loading, the trap column was switched on-line to a PepMap RSLC C18, 2 μm, 75 μm x 25 cm EasySpray column (Thermo Scientific). Peptides were then separated at low pH in the second dimension using a 7.5–30% ACN gradient over 90 min in mobile phase containing 0.1% formic acid at 300 nl/min flow rate. Each second-dimension LC run required 2 h for separation and re-equilibration, so each 2D LC-MS/MS method required 18 h for completion. Tandem mass spectrometry data was collected using an Orbitrap Fusion Tribrid instrument configured with an EasySpray NanoSource (Thermo Scientific). Survey scans were performed in the Orbitrap mass analyzer (resolution = 120,000), and data-dependent MS2 scans performed in the linear ion trap using collision-induced dissociation (normalized collision energy = 35) following isolation with the instrument's quadrupole. Reporter ion detection was performed in the Orbitrap mass analyzer (resolution = 60,000) using MS3 scans following synchronous precursor isolation of the top 10 ions in the linear ion trap, and higher-energy collisional dissociation in the ion-routing multipole (normalized collision energy = 65).

TMT Data Analysis—RAW instrument files were processed using Proteome Discoverer (PD) version 1.4.1.14 (Thermo Scientific). For each of the TMT experiments, raw files from the 9 fractions were merged and searched with the SEQUEST HT search engine with a *Mus musculus* Swiss-Prot protein database downloaded July 2015 (16,716 entries). Searches were configured with static modifications for the TMT reagents (+229.163 Da) on lysines and N termini, carbamidomethyl (+57.021 Da) on cysteines, dynamic modifications for oxidation of methionine residues (+15.9949 Da), parent ion tolerance of 1.25 Da, fragment mass tolerance of 1.0005 Da, monoisotopic masses, and trypsin cleavage (max 2 missed cleavages). The large parent ion tolerance was used to increase the number of peptides being scored to improve discrimination of true *versus* false identifications (24). Searches used a reversed sequence decoy strategy to control peptide false discovery and identifications were validated by Percolator software (25). Protein false discovery rate (FDR) estimates are unavailable in PD 1.4, but we expect protein FDR to be very low because we are quantifying the intersection of identifications from three TMT sets. Only peptides with q scores ≤ 0.05 were accepted, and at least one unique peptide was required for matching a protein entry for its identification.

Search results and TMT reporter ion intensities were exported as text files and processed with in-house scripts. A median reporter ion intensity peak height cutoff of 700 was used, and all reporter ion intensities for unique peptides matched to each respective protein were summed to create total protein intensities. We employed two

normalization procedures to handle the 30-plex experiment (3 TMT experiments with 10 channels each). The first was applied within each 10-plex experiment. The grand total reporter ion intensity for each channel was multiplied by global scaling factors to adjust its total intensity to the average total intensity across the 10 channels. This corrects for small sample loading and labeling reaction efficiency differences.

MS2 scans are selected stochastically by the mass spectrometer for each peptide. Two identical peptides in two different TMT experiments having identical concentrations would be extremely unlikely to have similar reporter ion signals, because their sampled intensities would depend on the peptide concentration at the time of MS2 sequencing. Therefore, common, pooled internal standards were used to normalize reporter ion intensities of proteins between different TMT experiments. This allowed preservation of individual intensity-scale measurements and avoided calculation of relative intensity measures such as ratios or percentages within each TMT experiment. To accomplish this, the duplicate summed reporter ion measurements for each protein in the common pool channels within each TMT experiment were averaged and used to create reference values for each protein. The three reference values for each protein in each TMT experiment were then averaged (geometric mean), and scaling factors calculated for each protein to adjust its reference value to the geometric mean value. These scaling factors were then used to adjust the summed reporter ion intensities for each protein in the remaining eight experimental samples in each TMT experiment. We call this procedure internal reference scaling (IRS).

Differential protein abundance between groups was then determined by comparing the IRS-normalized total reporter ion intensities between groups using the Bioconductor package edgeR (26), which uses quasi negative binomial and the quantile-adjusted conditional maximum likelihood (qCML) method for experiments with single factor. Additional data normalizations, multiple testing corrections, and calculation of false discovery rates were performed within edgeR.

Western Blotting Antibodies—Antibodies were purchased from Proteintech: ENO3 (16421–1-AP); Novus Biologicals: ECM1 (AF4428-SP), YAP1 (NB110–58358SS); Abcam: β-actin (ab8227), Vinculin (ab129002), Thermo Fisher: ACLY (PA5–29495), and Sigma: rabbit IgG (A0545), goat IgG (A8919). Equal amounts of epididymal adipose protein samples (20 μg) were subjected to NuPAGE 4–12% Bis-Tris gels for electrophoresis and transferred to nitrocellulose (0.45 μm). Membranes were blocked with 3% nonfat dry milk in TBS-T (10 mM Tris-HCl, 150 mM NaCl, 0.1% Tween 20, pH 7.6) for 2 h at room temperature. The membranes were probed with primary antibody overnight at 4 °C. After washing with TBS-T, the membranes were incubated with the appropriate HRP conjugated secondary antibody for 2 h at room temperature. After washing with TBS-T, the membranes were incubated with chemiluminescent HRP substrate. Western blots were imaged by scanning with the C-DiGit blot scanner (Li-Cor, NE) and analyzed using Image J software (NIH). β-actin or vinculin was used as a loading controls.

Bayesian Gene Regulatory Networks in Mouse Adipose—To retrieve gene-level relations of the protein signatures detected in the study, we utilized Bayesian network models reconstructed from adipose gene expression data from multiple previously published human and mouse studies each involving genetics and gene expression data from hundreds of samples (1–5), using an established method (27, 28). A consensus adipose network was derived from the individual networks by including only network nodes and edges that are present in networks from at least two studies.

Key Driver Analysis to Prioritize Central Regulators of Gene Signatures—We applied a key driver algorithm (27, 29–31) that maps the mouse protein signatures from the current study to the adipose gene regulatory network described above to identify the potential key regulatory genes. In this case, we defined a key driver as a gene that is connected to large numbers of genes encoding the protein signatures, compared with the expected number of neighboring protein signatures for a randomly selected gene within a network. Statistical significance was determined using the Fisher's exact test and multiple testing corrections were applied using the Benjamini-Hochberg FDR method (32). In this analysis, adipose gene regulatory networks rather than protein-protein interaction networks are used, because protein-protein interaction is not required for functionally related proteins to execute their function. In contrast, regulatory networks better capture the functional relatedness and relations among genes and proteins.

Statistical Analyses—Phenotypic data were represented as means ± S.E., ANOVA with Tukey post hoc correction was used. Detailed statistics for each analysis is described in the corresponding sections.

Data Availability—The mass spectrometry proteomics data have been deposited to the ProteomeXchange Consortium via the PRIDE (33) partner repository with the data set identifier PXD005953.

RESULTS

Strategies to Increase Sample Size and Probe Protein Variation in Adipose Tissue—We designed an experimental approach that allowed us to examine the proteome changes in response to short-term and long-term high fat diet, and age-related changes either on low-fat or high-fat diet (Summarized in Fig. 1*A*). We randomized our samples (five mice from four groups) across three 10-plex TMT experiments and included 2 identical pooled samples (A and B) in each TMT 10-plex analysis (Fig. 1*B*). First, we adjusted each sample to the average total reporter ion intensity within each TMT experiment to control for small differences in peptide concentrations and labeling efficiencies, both by adjusting volumes of each TMT labeling reaction prior to the 2D LC-MS/MS analysis and afterward in software during analysis steps. This traditional normalization strategy uses single multiplicative factors for each reporter ion channel.

We also developed a novel normalization method to correct for the random sampling of parent ions across multiple LC-MS/MS runs that placed each protein on a common reporter ion intensity scale across all three TMT experiments (see Fig. 1*C*). We used a common pooled internal standard labeled with two TMT reagents within each TMT experiment to create internal references for each protein that could be matched between the TMT experiments. The scaling factors that put the references on a common intensity scale were applied to all reporter ion channels for each protein in its respective TMT experiment. We call this method Internal Reference Scaling (IRS), and a more detailed description is available via the Supplemental file "IRS Normalization Method".

The IRS method uses standard analysis steps within each TMT run: contaminants and nonunique peptides are excluded and total protein intensities are computed from all associated unique peptides. The grand total of all intensities for each reporter ion channel are matched between the ten channels with each TMT run. After this processing is done for each TMT run, the duplicate measures of the proteins in the pooled standard are averaged within each TMT run. Geometric

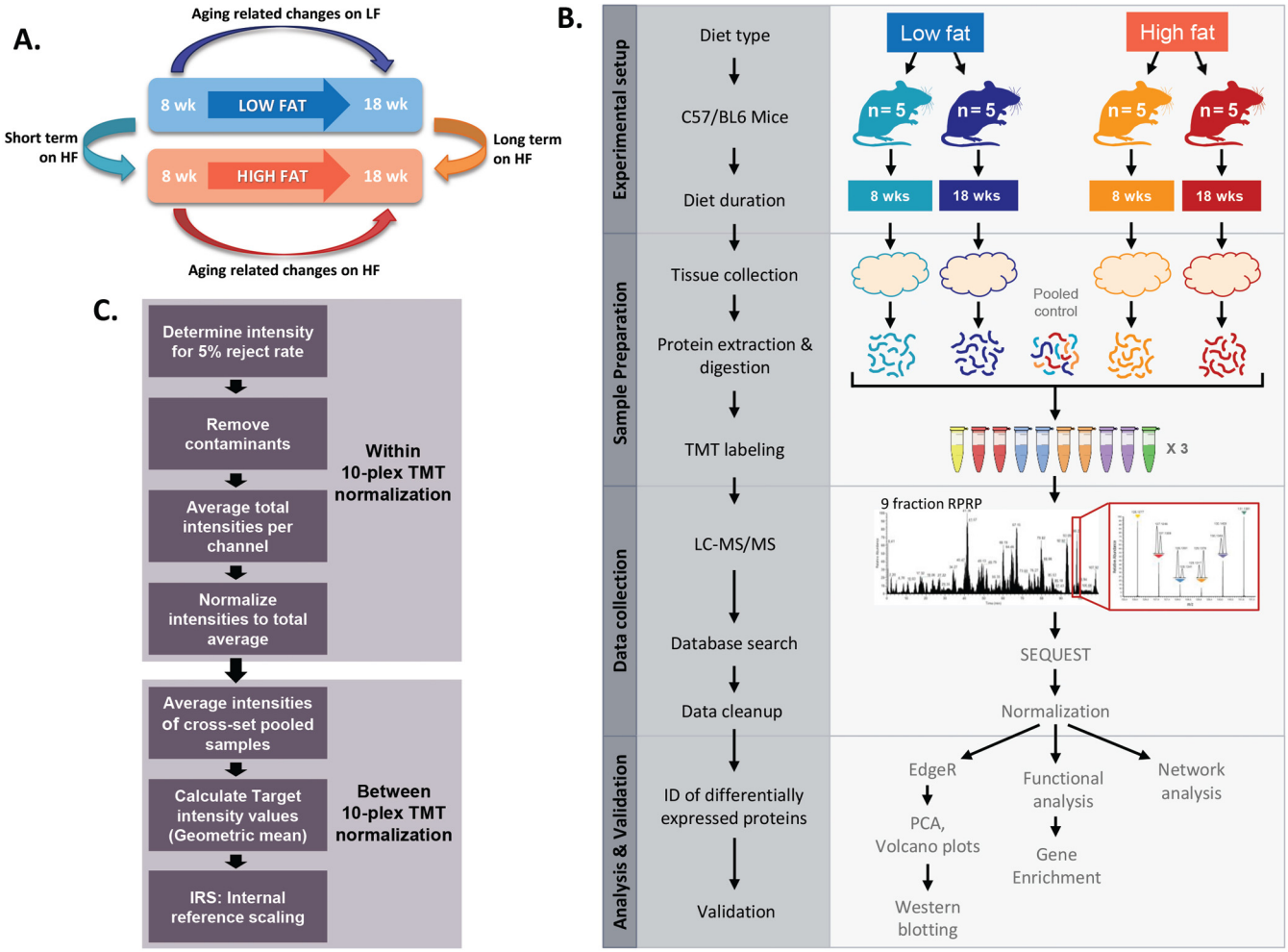

FIG. 1. **Experimental setup and workflow for comparison of diet and age related changes in epididymal adipose proteome.** *A*, Changes related to age were determined by comparing short term and long term diets within the same diet type, whereas short term and long term changes because of diet were determined by comparing the different diets for the same duration. *B*, Twenty mice at 8 weeks of age were placed on either low fat or high fat diets for either a short (8 weeks) or long (18 weeks) duration (5 mice per experimental group). Epididymal adipose was collected, lysed, and 100 mg subjected to trypsin digestion. Peptides from each individual sample, and from pooled internal reference samples, were randomly distributed and labeled across three TMT experiments. Following labeling, samples were pooled within their TMT experiment and separated with nine fraction two-dimensional reverse phase chromatography. Tandem mass spectrometry data were collected on the Orbitrap Fusion and proteins identified using Proteome Discoverer. *C*, Reporter ion intensities were processed and normalized first within TMT experiments and then across TMT experiments using internal reference scaling (IRS) normalization. *D*, Differentially expressed proteins were determined through group comparisons in edgeR and further characterized through gene enrichment and network analysis. Representative proteins were validated with Western blotting.

means of all averaged pooled standard protein measures between all TMT runs are then calculated. These mean intensities are the reference intensity values for each protein and used to compute the IRS factors. Only proteins observed in all TMT experiments (intersection of protein identifications) can be quantified with this method; therefore, some decrease in the number of quantifiable proteins occurs with each additional TMT experiment.

Once the pooled standard intensities have been determined for each protein in each TMT experiment in the study, adjustment factors can be computed that scale the pooled standard intensities to the reference values. The procedure is shown schematically in supplemental Fig. S1. These factors are also used to scale the 8 nonpooled standard channel intensities for each protein. Scaling factors are applied within each TMT experiment for each protein. After IRS normalization, individual reporter ion intensities can be directly compared between TMT experiments using standard statistical testing.

IRS normalization makes the value of a particular reference protein's abundance estimate measured in different TMT experiments the same between TMT experiments. The individual proteins present in the pooled standards are always at the same abundance in each TMT experiment that are part of the larger biological experiment. It stands to reason that different

measurements of the same thing should give the same answer. The IRS method corrects instrumental measurement differences between TMT experiments.

The IRS procedure described here incorporates two important quality controls. One is to use an average of two duplicate measurements in each TMT experiment to provide a better abundance estimate. The other is to apply the method at the protein level rather than the PSM level. Wenger *et al.* show that summing PSM signals to create protein signals improves the accuracy and precision (34). The scaling factors in IRS are derived from the pooled standard data only, but, because of the nature of multiplexing in TMT experiments, can be applied to the other 8 biological samples.

To validate the IRS normalization method, we performed an alternate analysis where we used a single measurement of a common reference sample (A) in each plex to IRS normalize across the three batches and checked the results by examining the unused common reference sample (B) in each plex. Both A and B references were created from the same pooled material. The geometric means of the three samples (A) from each TMT-plex were calculated for each protein. Scaling factors for all reporter ion channels for each protein within individual TMT experiments were calculated and used to adjust the summed reporter ion intensities for each respective protein (supplemental Fig. S1). The effect of normalization was monitored by: 1) the correlation of the sample (B) between the 3 TMT runs both pre and post normalization (supplemental Figs. S2*A*–S2*F*), the changes in widths of expression ratio distributions (supplemental Figs. S3*A*–S3*F*), and the CVs pre and post normalization when comparing proteins in sample B across the 3 TMT runs (supplemental Figs. S4*A* and S4*B*). All metrics showed dramatic improvements after IRS normalization. Note that the actual IRS procedure used on the experimental data computed the averages of both samples A and B of the pooled internal standard and this would further have improved the IRS normalization procedure across TMT runs.

Metabolic Parameters Worsen With High Fat Diet—To develop our proteome method, we used epididymal adipose tissues from mice that were on high fat diet either for 8 or 18 weeks (Fig. 1). To confirm the shift in their metabolic status, we measured body weight, epididymal depot weight, adiposity, fasting plasma glucose, insulin, total cholesterol and triglycerides (Figs. 2*A*–2*G*). The gradual impairment of glucose homeostasis because of aging or high fat diet was confirmed by glucose and insulin tolerance tests (Figs. 2*H* and 2*I*).

At the time of sacrifice, the body weights of mice from short-term *versus* long-term and low fat *versus* high fat fed groups were significantly different. ANOVA analysis captured significant effects of both diet and duration on both body weight and adiposity (Figs. 2*A* and 2*C*, $p < 0.0001$). Even though the body weights of short-term high fat fed mice were comparable to the long-term low fat fed mice, they had significantly increased abdominal adipose depot weights (Fig. 2*B*, 0.36 ± 0.11 g *vs.* 1.38 ± 0.41 g, $p < 0.001$), confirming that our experimental groups were significantly different in their adipose tissue weight.

Fasting plasma glucose (Fig. 2*D*), insulin (Fig. 2*E*), and total cholesterol (Fig. 2*F*) levels gradually worsened following the group order of short term low-fat (the most favorable), long-term low fat, short-term high fat, and long term high fat diet (the least favorable). Plasma triglycerides levels (Fig. 2*G*) were the lowest in long-term low fat diet group and gradually increased in short and long term high-fat feeding.

Glucose tolerance tests were comparable for low-fat diet fed mice for either 8 weeks or 18 weeks (Fig. 2*H*). Both short and long-term high fat feeding led to impaired glucose tolerance. Insulin tolerance test was comparable for low-fat fed groups, but was impaired in mice that were fed high-fat diet for longer time (Fig. 2*I*). Collectively, elevated fasting plasma glucose, insulin, cholesterol, and triglycerides levels with a gradual worsening of glucose tolerance profiles indicated development of impaired glucose tolerance as early as 8 weeks of high fat diet that is overtly present by 18 weeks of high fat feeding. These measurements confirmed that diet challenge was successful and indicated distinct peripheral metabolic status for each group.

Proteome Profiling Overview of Adipose Tissue—The cluster heatmap analysis, using unsupervised hierarchical clustering with a Pearson correlation, separated the experimental groups by diet and diet duration (Fig. 3*A*). Short-term high fat fed mice displayed a poor clustering pattern and were distributed into other groups. This suggests that metabolic response to short term high fat feeding results in a wide array of dynamic changes in the adipose tissue proteome causing greater biological variability. The fact that our biological parameters (diet, duration, experimental groups) clustered closely and the technical parameter (batch numbers) did not cluster indicates that our method can yield meaningful biological information.

We identified a total of 4678 proteins, with an average of 3550 per TMT experiment which more than doubles the number of identified adipose tissue proteins in previous reports (Fig. 3*B*) (9, 13). A full statistical analysis containing all biological replicates can only be applied to proteins observed in all TMT experiments so the quantifiable protein list was reduced to 2547 (supplemental Table S1). Each experimental group comparison followed a normal distribution with a similar number of up and down regulated differential expression candidates in each group. Histograms of the $\log_2$-transformed fold changes of each comparison: short-term high fat diet (8 week low *versus* high fat diet); long term high fat diet (18 week low fat *versus* high fat diet); age related changes on low fat (8 weeks low fat diet *versus* 18 weeks low fat diet); and age related changes on high fat diet (8 weeks on high fat *versus* 18 weeks on high fat diet) confirmed that the largest variations were associated with long term high fat diet feeding and with age-related changes on high fat diet groups (Figs. 4*A* and 4*B*). This suggests that long-term high fat feeding leads to a robust

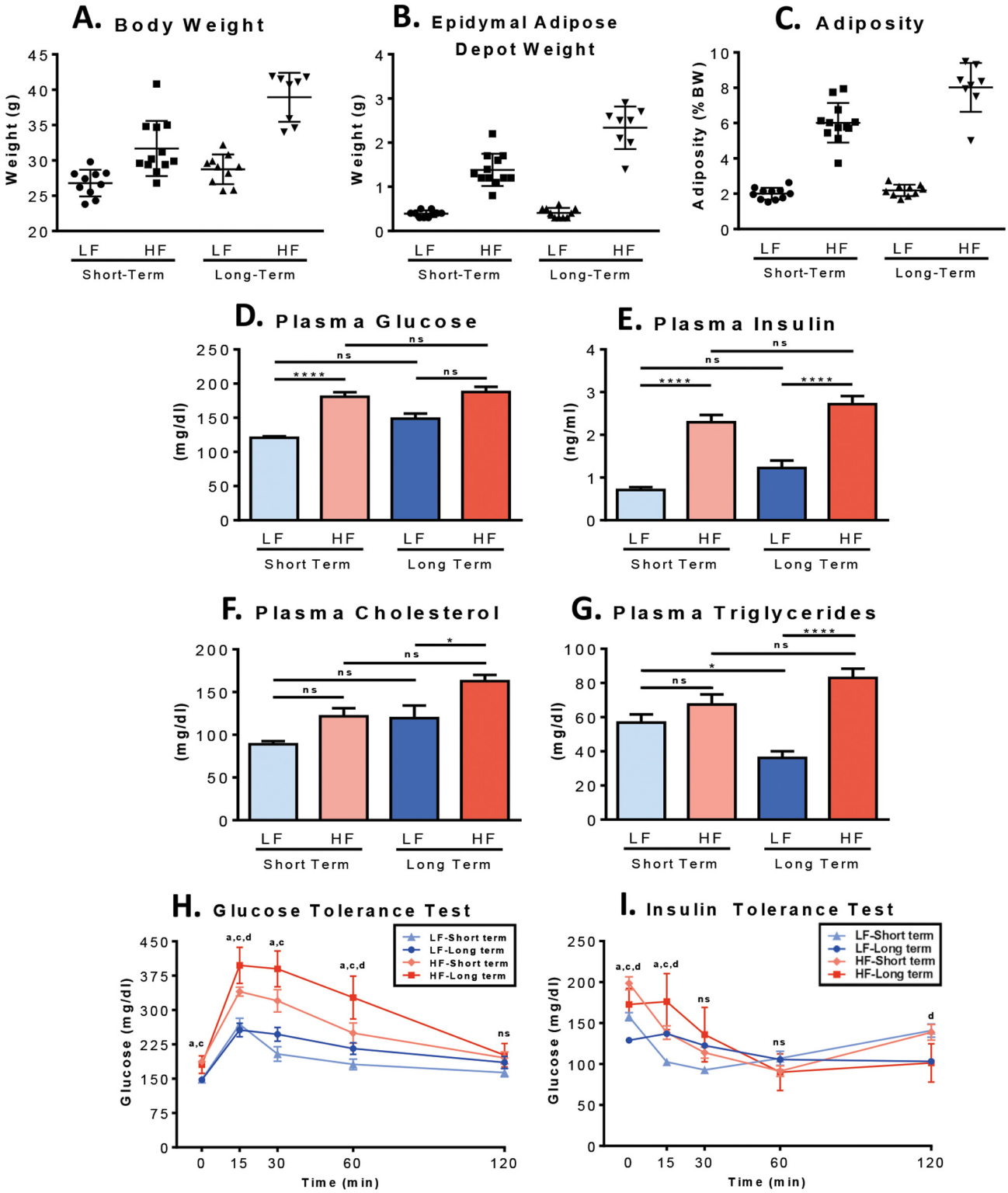

FIG. 2. **Metabolic parameters.** All measurements were taken from mice on short-term or long-term low fat (LF) or high fat (HF) diets. Body weight (*A*) and epididymal adipose weight (*B*) were measured at the time of collection and used to determine adiposity (*C*): short-term low fat $n = 10$, short term high fat $n = 12$, long-term low fat $n = 10$, long-term high fat $n = 8$. *D*, Plasma glucose levels measured after a 16 h fast: short-term low fat $n = 10$, short term high fat $n = 8$, long-term low fat $n = 31$, long-term high fat $n = 13$. Plasma insulin (*E*), cholesterol (*F*), and triglycerides (*G*) were measured at the time of sacrifice, after a 4 h fast. For both triglycerides and insulin measurements: short-term low fat $n = 11$, short term high fat $n = 8$, long-term low fat $n = 12$, long-term high fat $n = 8$. For cholesterol: short-term low fat $n = 11$, short term

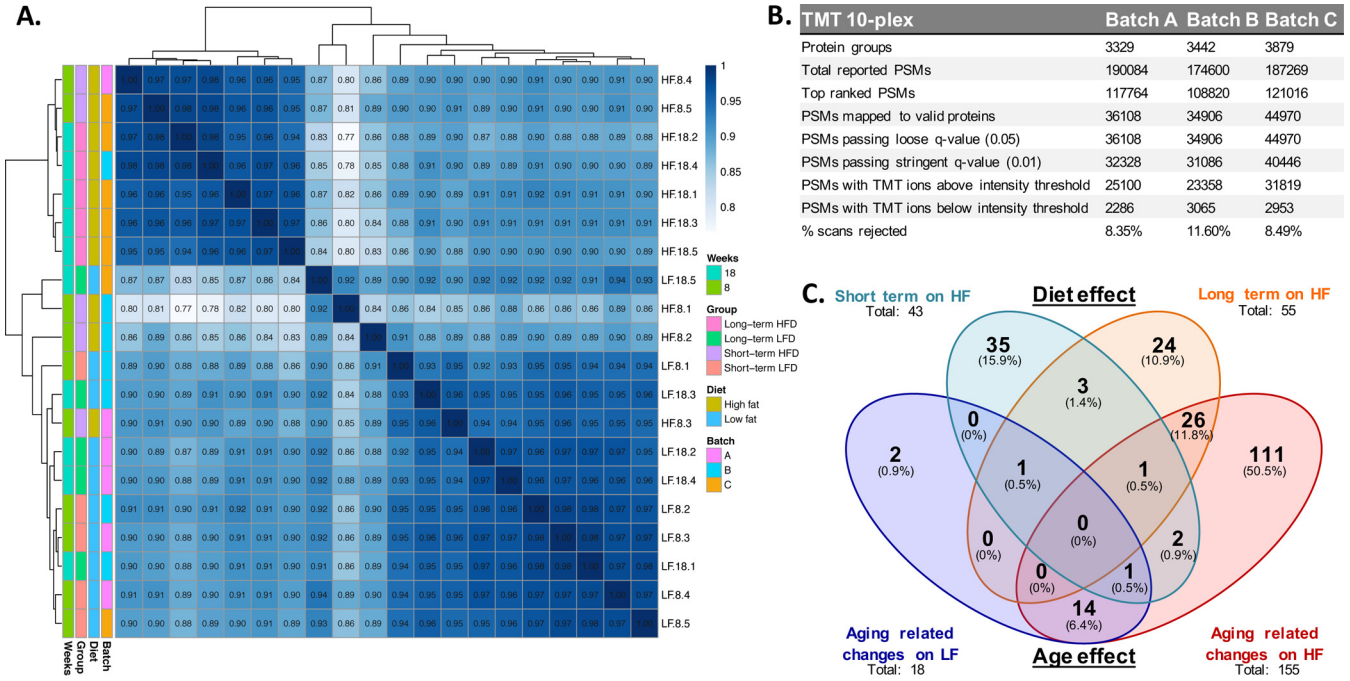

B.

TMT 10-plex	Batch A	Batch B	Batch C
Protein groups	3329	3442	3879
Total reported PSMs	190084	174600	187269
Top ranked PSMs	117764	108820	121016
PSMs mapped to valid proteins	36108	34906	44970
PSMs passing loose q-value (0.05)	36108	34906	44970
PSMs passing stringent q-value (0.01)	32328	31086	40446
PSMs with TMT ions above intensity threshold	25100	23358	31819
PSMs with TMT ions below intensity threshold	2286	3065	2953
% scans rejected	8.35%	11.60%	8.49%

FIG. 3. **Sample acquisition and overview of data characteristics.** *A*, Sample cluster heatmap analysis was performed with hierarchical clustering using the Pearson correlation method. *B*, Results from each TMT experiment database search. *C*, Venn diagram of proteins with significantly different abundance (FDR < 0.1) from each experimental group comparison.

adipose tissue metabolic response associated with increased number of protein changes.

Metabolic State Specific Proteome Changes in Adipose Tissue—We used edgeR based on negative binomial distributions, including empirical Bayes estimation, exact tests, generalized linear models and quasi-likelihood tests (35) to determine the differentially expressed proteins. The underlying model in edgeR has be used on different types of data from spectral counting proteomics experiments (36, 37), to TMT data sets (38, 39). A recommended way to evaluate statistical model appropriateness in differential expression omics experiments (where most genes/proteins do not have any differential expression) is to plot the distribution of raw *p* values (not corrected for multiple testing) (40). The raw *p* value distributions (supplemental Fig. S5) had the expected appearance of a flat *p* value distribution (for unchanged protein expression) with modest "spikes" at small *p* values for the differentially expressed proteins. We identified significantly changing proteins in all experimental groups: 18, 43, 55, and 155 differentially expressed proteins (see supplemental Figs. S6*A*–S6*D*) for age related changes on low-fat diet, short-term high fat diet, long term high fat diet, and advancing age on high fat diet groups, respectively (FDR < 0.1; Fig. 3*C*, and supplemental Table S1). Of these proteins, 2/18, 35/43, 24/55, 122/156 were unique to their corresponding experimental groups (supplemental Table S1).

The distributions of statistical significance (-log adjusted *p* values) and magnitude of change (Log_2 fold change) for all the proteins for each group are represented by volcano plots (Figs. 4*C*–4*F*). Large numbers of proteins in each group varied greater than 2-fold without satisfying the stringent criteria of FDR < 0.1.

Validation of Proteomic Signals by Protein Immunoblots—To validate our proteomic approach, we compared, in Fig. 5, the expression levels of proteins measured by proteomics (TMT reporter ion intensities, Fig. 5*A*) and Western blot (immunostaining, Fig. 5*B*). The Western blots are shown in supplemental Fig. S7. When choosing the proteins to validate, we selected proteins represented by high and low ion intensities and either reaching statistical significance or missing it by a margin. ACLY (FDR = 2.11E^-10, 25th percentile abundance), YAP1 (FDR = 0.0586, 25th percentile abundance),

high fat $n = 11$, long-term low fat $n = 12$, long-term high fat $n = 8$. Insulin (*H*) and glucose tolerance (*I*) tests were performed after a 4 h fast. For insulin tolerance tests: short-term low fat $n = 12$, short term high fat $n = 16$, long-term low fat $n = 8$, long-term high fat $n = 10$. For glucose tolerance tests: short-term low fat $n = 9$, short term high fat $n = 13$, long-term low fat $n = 8$, long-term high fat $n = 8$. All error bars are standard error of the mean. Significance was determined by ANOVA followed by a Tukey's posthoc analysis for multiple comparisons. For D–G significance is indicated as * for $p < 0.05$, **** for $p < 0.0001$, ns for not significant. For H-I significance is indicated as (a), short-term HF *versus* Long-term HF; (c), short-term LF *versus* long-term LF; (d), short-term LF *versus* short-term HF; an (ns), not significant. All error bars are standard error of the mean.

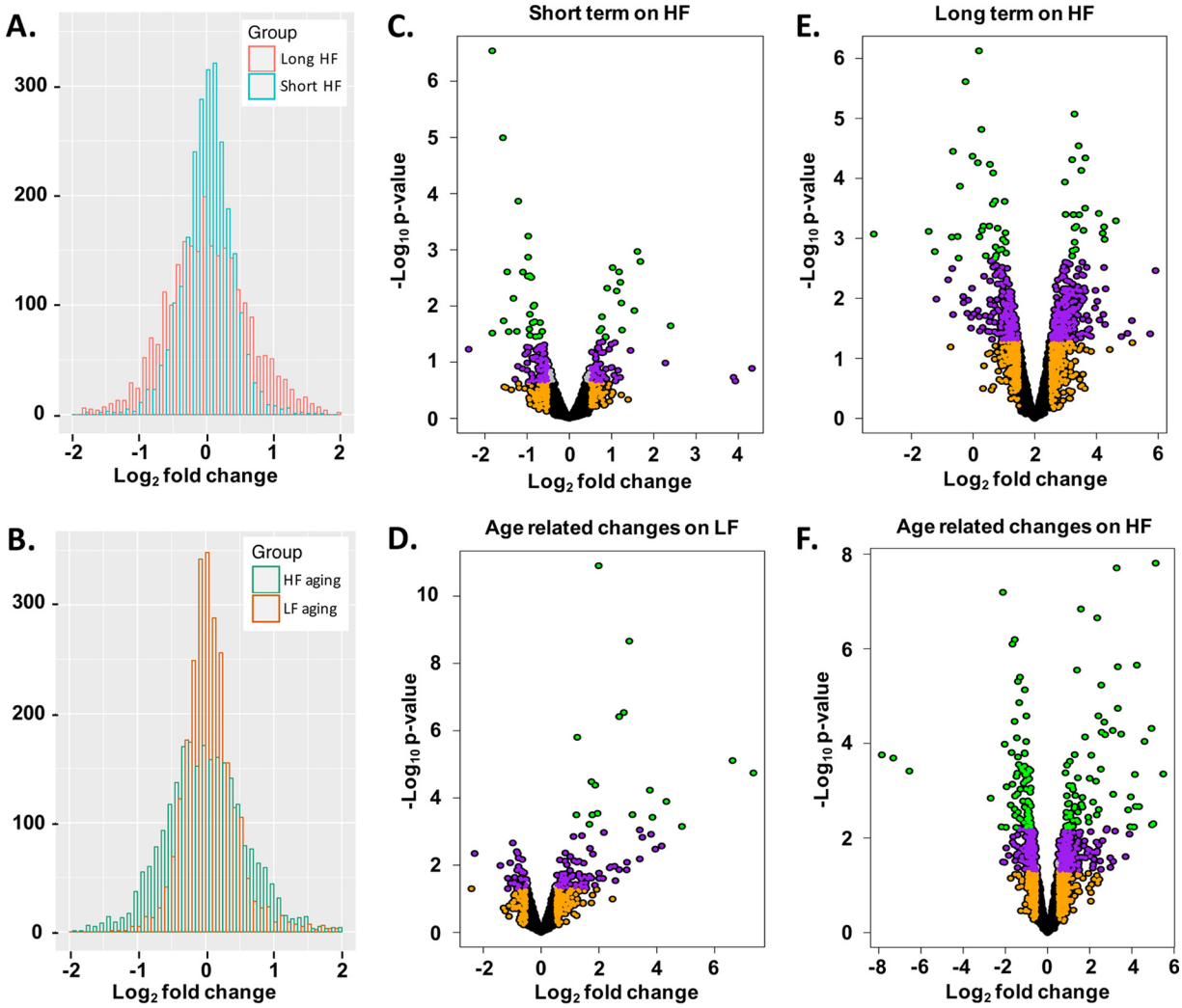

FIG. 4. **Fold change distribution in comparisons.** Log fold-change distribution histograms comparing (*A*) long-term high fat diet to short-term high fat diet, and (*B*) long-term high fat diet to long-term low fat diet. *C–F,* Volcano plots from different group comparisons. Gray points represent samples with $p < 0.05$, orange represent $\log_2$ fold change > 0.5, purple represent both a $\log_2$ fold change > 0.5 and $p < 0.05$, and green points represent an adjusted $p < 0.1$ and a $\log_2$ fold change > 0.5.

ENO3 (FDR = 0.2232, 75th percentile), ECM1 (FDR = 0.0242, 50th) were used to validate results from short-term high fat diet, long term high fat diet, age related on low fat diet, and age related on high fat diet groups, respectively (Fig. 5). The quantification of the relative expression levels of all the proteins by Western blot followed the expression level and significance trends identified by TMT quantification.

Proteome Changes Capture Metabolic State Specific Biologic Pathways—Short-term and long-term high fat diets resulted in comparable numbers of altered proteins (43 and 55, respectively). However, the pathways these proteins are associated with are different. Gene enrichment analyses using the gene ontologies from online curated databases DAVID/EASE (https://david.ncifcrf.gov), Panther (http://pantherdb.org), and STRING (http://string-db.org) (41) for the significantly changed proteins identified diverse biological pathways representing the metabolic changes in adipose tissue in response to high fat diet. We have compiled the data from the three different gene ontology databases and represent the biological pathways that are represented by at least two genes in Figs. 6*A*–6*D*. The enrichment tables from DAVID are also presented in supplemental Table S2.

Short-term high fat diet led to alterations in proteins contributing to lipid metabolism (*i.e.* ACLY, AACS, ACSM5), highlighting fatty acid synthesis (ACACA, ACACB, FASN), redox pathways (SOD3, ALDH4a1, ALDH6a1, CYP2E1), mitochondrial metabolism related protein (PDHB, ALDH2, MPST, SUCLG2), and proteins associated with cytoskeletal structure and assembly (SYNOP2, MAP1A, TUBB2, PALMD, VIM, TUBB6 (Fig. 6*A*). All the proteins that participate to cytoskeletal functions are downregulated. All the proteins that associate with oxidoreductase activity are significantly up-regulated except for SOD3 (Table I). SOD3 is an extracellular dismutase with strong antioxidant activity and has been pre-

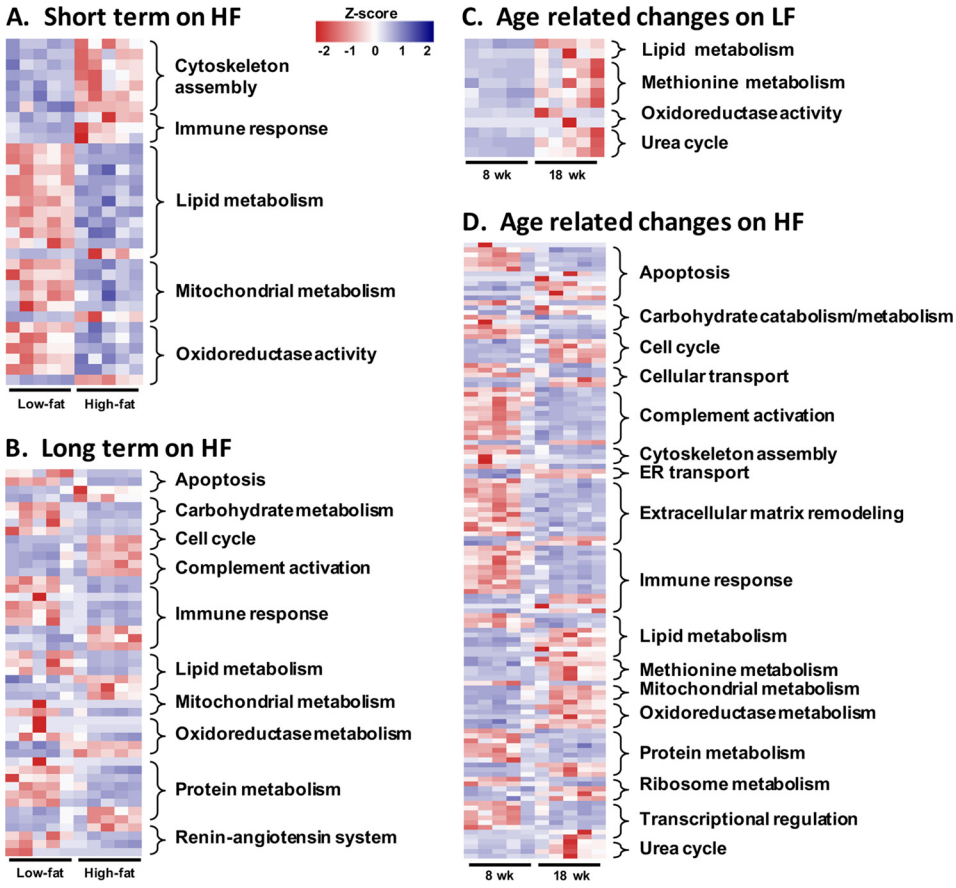

FIG. 5. **Visualization of changing proteins and their biological pathways.** *A–D*, Gene enrichment analysis was performed for proteins with FDR > 0.1, with DAVID/EASE, PANTHER, KEGG, and STRING databases. Functional categories were compiled and heatmaps generated from categories containing 2 or more protein groups.

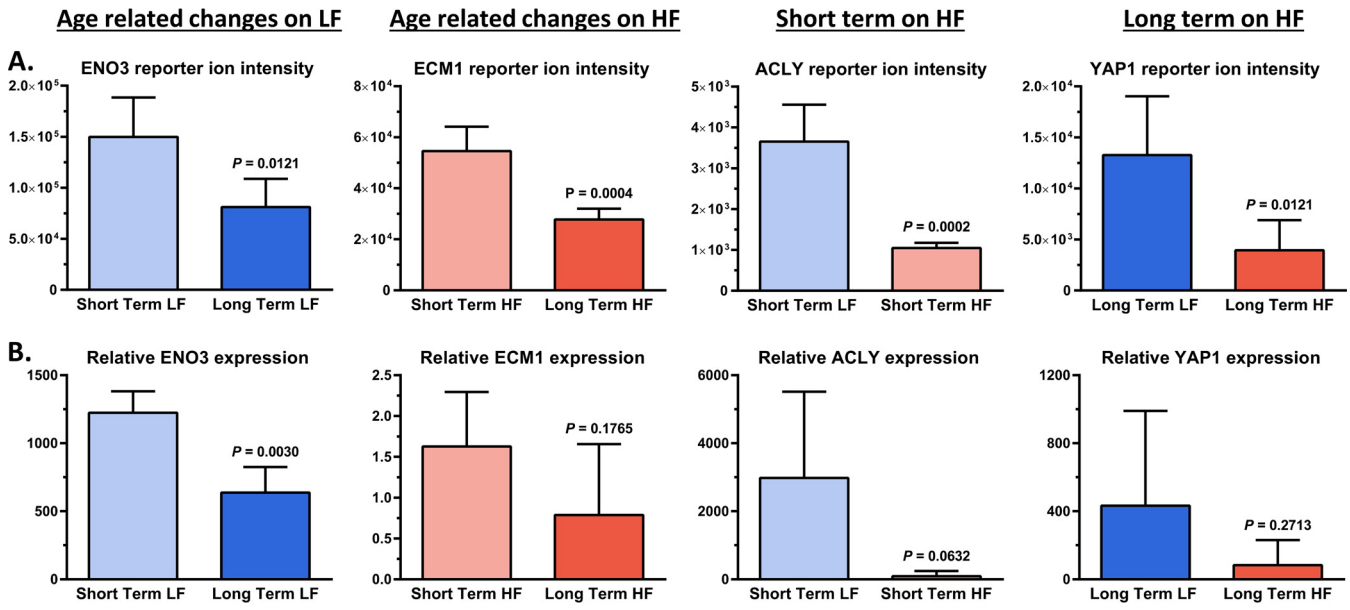

FIG. 6. **Comparison of expression level measurements.** *A*, Representative proteins from each group comparison were blotted from epididymal adipose tissue cell lysate. Loading controls were used to determine relative expression through analysis with ImageJ software. *B*, The reporter ion intensities for the blotted proteins were also plotted for comparison. All plots are mean with the standard error of the mean, and are analyzed using Student's *t* test.

viously shown in adipocytes to protect against hyperglycemia induced reactive oxygen species (42). Short term high fat feeding impaired glucose homeostasis as shown by increases in plasma glucose (30%), insulin (2.5-fold), and cholesterol (30%) levels (Figs. 2*D*–2*I*). Reduced insulin sensitivity is likely to engage adaptive cellular responses to nutrient usage. Down-regulation of the nutrient associated pathways in adipose tissue seems to reflect the reduced peripheral insulin sensitivity, and could represent a transient protective cellular metabolic response.

Long-term high fat diet led to changes in the proteins involved in the immune system (GC, SYK, SHARPIN, IL1RAP, LCP1, PTGES), complement activation (ANXA5, C4b, CSTB, CFD), renin angiotensin system (ANPEP, ENPEP, CMA1, CPA3), and protein synthesis (ANXA1, EEF2K, HOOK2, DYNC1LI1, NOP58) (Table I and Fig. 5*B*). 6 out of 12 immune response and complement activation proteins, SYK, LCP1, ANXA1, ANXA5, and CSTB are up-regulated. SYK (tyrosine kinase) activates NF-kappa-B mediated transcription of cytokines and chemokines, and stimulates ROS production from immune cells (43, 44) and its transcription has been shown to be elevated in obese insulin resistant subjects (45). We also see this protein expression increased in obese insulin resistant mice. PTGES, prostaglandin E synthase 2, is involved in prostaglandin biosynthesis that is reactive to inflammation, NF-κB is involved in the regulation of *Ptges* expression (46). In addition, its gene expression has been shown to be down regulated in macrophages in response to glucose treatment (47). Concordantly, we observe reduced PTGES levels in hyperglycemic insulin resistant mice. Further, angiotensin 2 inhibition leads to adipose tissue enlargement and insulin resistance (48, 49). Down-regulation of renin angiotensin system enzymes CPA3, EGFR, ENPEP, and ANPEP leads to reductions in angiotensin 2, 3, and 4, respectively. Collectively, these changes reflect adipose tissues adaptive responses to obesity and insulin resistance.

Adipose tissue response to high fat feeding includes up-regulation of inflammatory markers (50). Because we did not detect inflammation related protein changes in short term fed group, we looked at gene expression levels of four commonly measured cytokines, (TNF-α, IL-1-β, IL-6, and IL-12α) in whole adipose tissue (supplemental Fig. S8) in the group of mice that have been exposed to high fat diet longer. We observed no changes between the low-fat and the high fat fed group. In addition, we isolated the stromal vascular fraction (SVF) in an independent cohort of mice that were fed high fat diet for 8 weeks and measured the expression levels of the same cytokine genes, and did not observe any differences between the low-fat fed and high fat fed groups (supplemental Fig. S9). Despite development of glucose intolerance and mild dyslipidemia, proteomic analysis of the whole adipose tissue and gene expression levels of common proinflammatory cytokines do not support the presence of inflammation in whole adipose tissue at 8 and 18 weeks of high fat diet.

Age-related changes on low fat diet are represented by up-regulation of urea (ASS1, OTC, CPS1, ABP1), methionine and amino acid metabolism (MAT1A, ALDOB, CTH, BHMT), all of which are part of tissue aging related responses (Table I and Fig. 6*C*). Mutations in Aldob have been implicated in serious defects of fructose metabolism (51). Meanwhile, Aldob responds to low-calorie diet with changes in insulin secretion and gene expression in subcutaneous adipose tissue (52). Mice lacking betaine-homocysteine methyltransferase (BHMT), enzymes that remethylates homocysteine to methionine, have increased energy expenditure and insulin sensitivity, and are resistant to diet-induced obesity (53). Collectively, the decline in peripheral insulin sensitivity observed with aging mice (Figs. 2*D*, 2*E*, 2*H*, and 2*I*) could be associated on adipose tissue level with up-regulation of methionine metabolism that impacts insulin sensitivity. Further studies are required to understand the impact of these pathways on adipose tissue metabolism.

Age-related changes on high fat diet led to more severe tissue responses where 155 significantly altered proteins participated primarily in urea cycle (OTC, ARG1, CPS1), immune response (ILIRAP, GC, ITIH4, CSDA, ARG1), complement activation (F2, C3, CFD, ABP1M, C8G, CF1, C4B, CFP), extracellular remodeling (EFEMP1, FBN1, FBN2, LTB4, FERMT2, ECM1, EMILIN2, ITIH3) and regulation of apoptosis (YAP1, HIP1, NDRG1, PRKCD, MUL1) (Table I and Fig. 6*D*). Increased metabolism of L-arginine by myeloid cells can result in the impairment of lymphocyte responses to antigen during immune responses that are triggered by prolonged high fat diet (54). The activation of myeloid cells result in the up-regulation of immune suppressive factors such as ARG1 (55). Down-regulation of eight complement activation proteins, interleukin 1 associated receptor (IL1RAP), acute phase inflammatory response protein (ITIH4), and vitamin D binding protein (GC) with chemotactic properties in inflammation suggests that we are capturing an innate immunity related component of immnune response. In light of large body of literature suggesting that aging is associated with inflammation (56, 57), our data suggest a complicated picture for the immune response in aging tissue with down-regulation of multiple proteins associated with complement activation. Further studies are required to elucidate the age related specific patterns of the immune response in adipose tissue. Collectively, these protein signatures describe an aging tissue with a strong stress response demonstrated by the dampening of a particular arm of immune response and activation of apoptosis.

Key Driver Network Analysis Identifies Diet and Age-related Specific Gene Networks in Response to Aging and High Fat Diet—To explore the relationships among the differentially expressed proteins in response to age and high fat diet, we conducted adipose gene network analysis to identify potential key regulators of the differential proteins and extracted the subnetworks that were perturbed by advancing age and high fat diet. For this type of analysis, use of small differential

TABLE I

Key differentially expressed proteins involved in important biological pathways. Protein column lists gene symbols, LogFC is the log, base 2, of the fold-change, FC is fold-change, FDR is the false discovery rate calculated by edgeR, Pathway: Biological pathway description, and Group: The experimental condition

Protein	LogFC	FC	FDR	Pathway	Group
ACLY	−1.83	−3.55	2.11E-10	Lipid Metabolism	Short-term High fat
AACS	−1.10	−2.14	0.0014	Lipid Metabolism	Short-term High fat
FASN	−1.21	−2.31	1.58E-05	Lipid Metabolism	Short-term High fat
ACSM5	−1.32	−2.50	0.0071	Lipid Metabolism	Short-term High fat
ACACA	−1.57	−2.97	1.31E-07	Carboxylic acid Biosynthesis	Short-term High fat
ACACB	−0.93	−1.91	0.0719	Carboxylic acid Biosynthesis	Short-term High fat
PC	−0.71	−1.63	0.0748	Carboxylic acid Biosynthesis	Short-term High fat
ALDH4A1	−0.83	−1.78	0.0112	Carboxylic acid Biosynthesis	Short-term High fat
CLPP	−0.64	−1.56	0.0564	Mitochondrial metabolism	Short-term High fat
IVD	−0.98	−1.98	0.0016	Mitochondrial metabolism	Short-term High fat
ALDH2	−0.97	−1.97	0.0002	Mitochondrial metabolism	Short-term High fat
SOD3	1.02	2.03	0.0014	Redox Pathways	Short-term High fat
UQCRH	−1.44	−2.71	0.0564	Redox Pathways	Short-term High fat
CYP2e1	−1.24	−2.36	0.0564	Redox Pathways	Short-term High fat
PDHB	−0.87	−1.83	0.0349	Redox Pathways	Short-term High fat
GC	−0.98	−1.97	0.0362	Immune system	Long-term High fat
SYK	1.33	2.51	0.0844	Immune system	Long-term High fat
SHARPIN	−2.69	−6.46	0.0623	Immune system	Long-term High fat
LCP1	1.21	2.32	0.0135	Immune system	Long-term High fat
IL1RAP	−1.29	−2.44	0.0362	Immune system	Long-term High fat
PTGES	−2.47	−5.54	0.0987	Immune system	Long-term High fat
ANXA5	1.22	2.33	0.0856	complement activation	Long-term High fat
C4B	−1.81	−3.51	0.0019	complement activation	Long-term High fat
CSTB	1.58	2.98	0.0587	complement activation	Long-term High fat
CFD	−1.59	−3.01	0.0941	complement activation	Long-term High fat
ANPEP	−0.95	−1.93	0.0598	Renin Angiotensin system	Long-term High fat
ENPEP	−0.93	−1.91	0.0889	Renin Angiotensin system	Long-term High fat
CMA1	−1.67	−3.18	0.0575	Renin Angiotensin system	Long-term High fat
CPA3	−1.79	−3.47	0.0623	Renin Angiotensin system	Long-term High fat
ANXA1	1.44	2.71	0.0448	Protein synthesis	Long-term High fat
EEF2K	−1.45	−2.74	0.0135	Protein synthesis	Long-term High fat
HOOK2	−3.24	−9.46	0.0864	Protein synthesis	Long-term High fat
DYNC1LI1	1.35	2.54	0.0575	Protein synthesis	Long-term High fat
NOP58	−1.73	−3.31	0.0098	Protein synthesis	Long-term High fat
ASS1	1.99	3.97	3.15E-08	Urea Cycle	Age related Low fat
OTC	1.74	3.33	0.0105	Urea Cycle	Age related Low fat
CPS1	3.05	8.27	2.77E-06	Urea Cycle	Age related Low fat
MAT1A	2.86	7.28	0.0002	Methionine metab	Age related Low fat
ALDOB	1.95	3.86	0.0542	Methionine metab	Age related Low fat
CTH	1.22	2.32	0.0542	Methionine metab	Age related Low fat
BHMT	1.67	3.18	0.0913	Methionine metab	Age related Low fat
OTC	2.30	4.92	0.0248	Urea cycle	Age Related High fat
ARG1	2.00	4.00	0.0229	Urea cycle	Age Related High fat
CPS1	2.56	5.92	0.0065	Urea cycle	Age Related High fat
IL1RAP	−1.40	−2.64	0.0010	immune response	Age Related High fat
GC	−1.08	−2.11	0.0013	immune response	Age Related High fat
ITIH4	−1.31	−2.47	0.0009	immune response	Age Related High fat
YBX3	−0.94	−1.91	0.0653	immune response	Age Related High fat
ARG1	2.00	4.00	0.0229	immune response	Age Related High fat
F2	−0.89	−1.85	0.0194	complement activation	Age Related High fat
C3	−0.87	−1.82	0.0230	complement activation	Age Related High fat
CFD	−1.66	−3.16	0.0003	complement activation	Age Related High fat
C8G	−1.02	−2.02	0.0320	complement activation	Age Related High fat
CFI	−0.86	−1.82	0.0334	complement activation	Age Related High fat
C4B	−2.12	−4.33	0.0001	complement activation	Age Related High fat
CFP	−1.34	−2.53	0.0023	complement activation	Age Related High fat
EFEMp1	−0.79	−1.73	0.0311	Extracellular Modelling	Age Related High fat

TABLE I—*continued*

Protein	LogFC	FC	FDR	Pathway	Group
FBN1	−1.07	−2.10	0.0127	Extracellular Modelling	Age Related High fat
FBN2	−1.10	−2.14	0.0198	Extracellular Modelling	Age Related High fat
LTBP4	−0.97	−1.96	0.0985	Extracellular Modelling	Age Related High fat
FERMT2	−0.79	−1.73	0.0563	Extracellular Modelling	Age Related High fat
ECM1	−0.95	−1.94	0.0242	Extracellular Modelling	Age Related High fat
EMILIN2	−1.40	−2.64	0.0133	Extracellular Modelling	Age Related High fat
ITIH3	−0.80	−1.75	0.0915	Extracellular Modelling	Age Related High fat
YAP1	−1.94	−3.84	0.0301	Apoptosis	Age Related High fat
HIP1	−0.88	−1.84	0.0664	Apoptosis	Age Related High fat
NDRG1	−1.01	−2.02	0.0081	Apoptosis	Age Related High fat
PRKCD	2.43	5.38	0.0614	Apoptosis	Age Related High fat
MUL1	4.93	30.51	0.0059	Apoptosis	Age Related High fat

protein signatures at stringent FDR cutoffs reduces statistical power and, for discovery purpose of singular proteins or biological pathways, relaxing the significance criteria is justified because the analysis does not rely on the accuracy of individual genes or proteins but their collective patterns. Therefore, we used differential proteins at a less stringent statistical cutoff, $p < 0.05$, without multiple testing corrections to enhance the statistical power. We applied a key driver analysis (KDA; details in Materials and Methods) to the differential protein candidates using adipose tissue-specific Bayesian network models constructed from transcriptomic and genetic data sets from multiple human and mouse studies (58–62), and identified 10–16 predicted putative key driver genes satisfying FDR < 0.05 in KDA for each metabolic state (supplemental Table S3).

Among the 218 differential candidates as part of short-term high fat diet related changes, 16 were identified as key driver genes (supplemental Table S3). In Fig. 7, metabolic status driven perturbations aligned with distinct gene subnetworks comprised of the top putative key drivers (we selected the top eight key driver genes from supplemental Table S3 for each category) and their neighboring differential candidates. Notable putative key driver genes included Mccc1, Pccb, and Hibadh, which are part of the branched-chain amino acid (BCAA) metabolism and participate in valine, leucine and isoleucine degradation (63). The protein amounts (TMT reporter ion intensities) decreased for all putative key driver genes except Ccbl2 (Supplemental Table 3), suggesting that short-term high fat feeding impairs BCAA metabolism. This is consistent with the previous observation that obesity and insulin resistance down regulate BCAA oxidation enzymes in adipose tissue (64).

Changes in response to long term high fat feeding and to advancing age on high fat feeding perturbed both shared and distinct networks. Two major shared networks are immune response and complement activation (C3, C2, C4b, C8a, Cfi, Serping1, Kng1, Hrg, Fgb, F2, Proc, Fermt3), and fatty acid metabolism (Cpt2, Hadhb Acat1, Acadsb). All protein products of the putative key driver genes associated with immune response significantly decreased in adipose tissues of the mice on fat high fat diet, except Fgb, while maturing (supplemental Table S3). On the other hand, the protein products of the key driver genes associated with fatty acid metabolism increased in older high fat diet fed mice. Our analysis captured an unprecedented decrease in proteins and gene networks associated with complement activation and macrophage activation and increase in proteins associated with fatty acid metabolism in older mice with prolonged high fat diet exposure. These data suggest a complex interaction between immune response and nutrient utilization in aging adipose tissue.

DISCUSSION

Obesity strongly contributes to diabetes and cardiovascular disease (65–67). Adipose tissue is the most plastic endocrine organ that plays a central role in energy homeostasis (68). Although the contribution of adipose tissue to obesity-related pathologies has been widely studied from the gene expression perspective (2–4), comprehensive protein level profiling is rare, primarily because of the lack of mature technologies and methods. Gene expression and protein expression diverge (16). Better tools to study alterations in adipose tissue proteomes are needed. In this study, we describe a reliable mass spectrometry method to highlight key proteins in adipose tissue that are modulated in response to metabolic shifts, and report proteomic signatures that are associated with duration of high fat diet and with the age-related changes in the tissue. By overlaying genomic, proteomic, and metabolic profiles, we identified diet and age related shifts in underappreciated pathways such as urea cycle, methionine and branch chain amino acid metabolism.

Studying the proteome of a complex tissue saturated with lipids is challenging especially when the tissue is limited such as in mice. Therefore, only a small number of groups have successfully studied the proteome of mouse adipose tissue (9, 13). Our novel approach takes advantage of highly multiplexed state-of-the-art isobaric labeling to reduce cost, and 2-D inline liquid chromatography separations to increase pro-

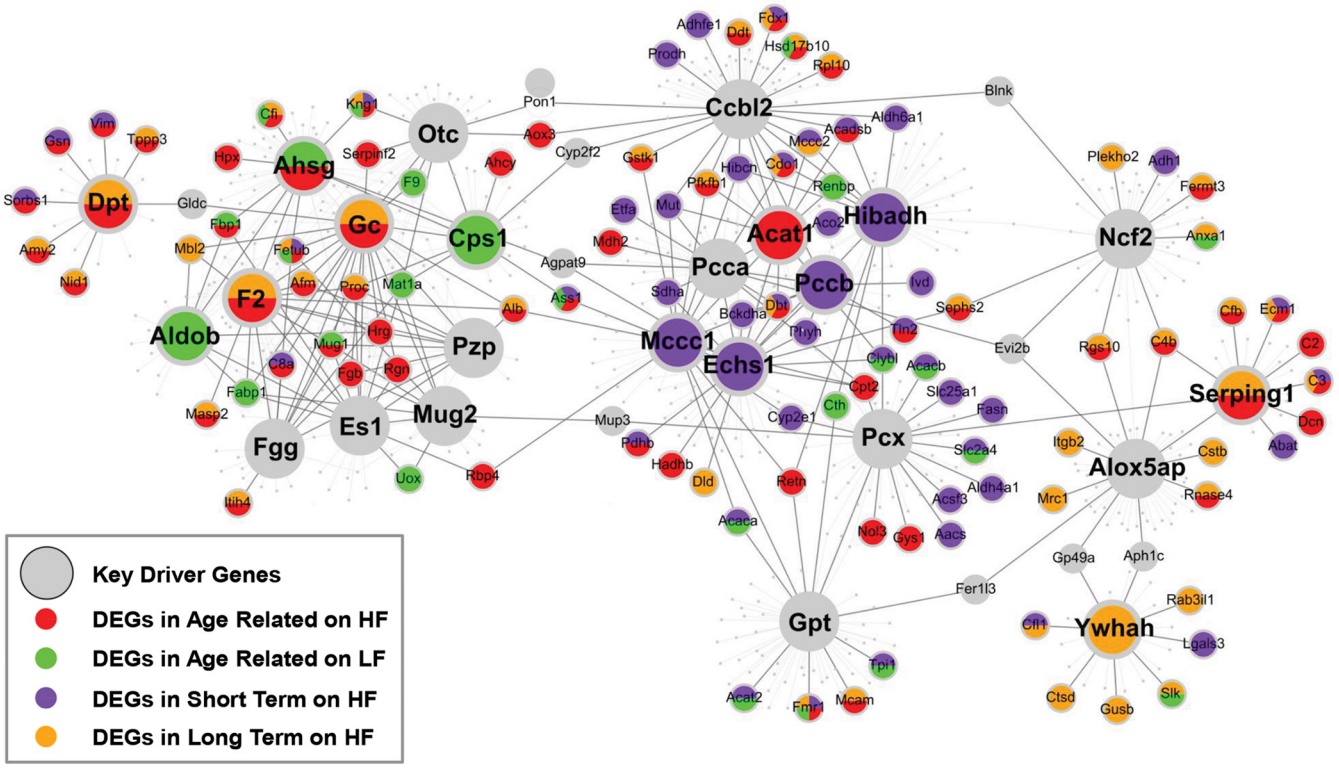

FIG. 7. **The top key driver genes in response to aging and high-fat diet in adipose.** The bigger nodes correspond to key driver genes whereas the different colors represent genes encoding protein signatures from different categories. The full list of key driver genes can be found in supplemental Table S3.

teomic profiling depth. Our findings agree with and greatly extend those from a recent publication using a similar approach with human tissue (11). A comparison of the proteins discovered between Gomez-Serrano *et al.* and our work revealed 1389 out of ~2500 shared proteins that participated in primary cellular pathways such as lipid metabolism, glycolysis, TCA cycle, and inflammation.

We present two major advances over previous techniques: (1) increasing the sample size by combining multiple 10-plex TMT sets, (2) using very low amounts of whole white adipose tissue (100 mg) because of the efficient protein isolation method that yields high protein extraction efficiency. This enables investigators to use multiple techniques such as flow cytometry and confocal microscopy in combination with omic techniques such as microarray and proteomics. We have also demonstrated an experimental design (pooled internal standards) and normalization strategy (IRS) that permit running multiple TMT plexes, which increases sample size (20 samples reported here) and discovery potential.

The 10-plex TMT methodology using synchronous precursor scans in the Orbitrap Fusion is precise and capable of measuring small expression differences in biological samples. The average median coefficient of variation for the pooled controls that were run on each TMT plex was 4.6%. This reflects the low proteomic methodological variability (trypsin digestion, TMT labeling, and instrumental reproducibility). The accuracy of TMT based experiments stems from having reporter ions from all samples measured simultaneously in the mass spectrometry for each labeled peptide, and this is born out in the low average median CV. Combining multiple TMT plexes could introduce variability and reduce the accuracy. In the IRS validation analysis, the median CV of the three pooled channels not used in the IRS procedure was only 8.3%, clearly demonstrating that multiple TMT experiments can be combined using the IRS procedure detailed here. The measurement dynamic range is also impressive with total protein intensities spanning five orders of magnitude.

The IRS normalization of total protein intensities offers important advantages compared with alternatives. Another way to utilize the pooled internal standard would be to compute the ratios of each sample reporter ion intensity to the average pooled standard intensity for each protein. Ratios have the disadvantage of reciprocal mathematical spaces where values are no longer symmetric. For example, under expression would result in ratios from zero to one, and over expression would have ratios from one to infinity. This asymmetry is often dealt with by taking the logarithm of the ratios. Although that takes care of the asymmetry, both ratio and logarithm calculations change the dynamic range of the values and the relationship between the mean and variance. Use of ratios is commonly done (often in $n = 1$ situations) and appropriate statistical testing can be performed. However, the IRS

method outlined here retains the observable data in its original intensity numerical space and avoids any nonlinear data transformations. Another advantage of our method comes from combining the individual MS3 reporter ion signals into single total protein intensities. This is akin to a weighted average as larger intensities contribute more to the total intensity and has been shown by others to improve quantification precision and accuracy (34).

Our experimental design allowed the dissociation of changes because of high fat feeding from those because of aging of the tissue. Age related changes on either low or high fat diet are captured by changes in amino acid biosynthesis such as methionine metabolism and urea cycle. The urea cycle, an essential pathway for the disposal of ammonia in mammals and many amphibian species, is comprised of five enzymes: carbamyl phosphate synthetase-I (CPS-I), ornithine transcarbamylase, argininosuccinate synthetase (ASS), argininosuccinate lyase (ASL), and arginase1 (69). MAT1A, methionine adenosyltransferase 1A, catalyzes the transfer of the adenosyl moiety of ATP to methionine to generate methyl groups. All of these proteins were altered in response to age: CPS1, MAT1A, and ARG1 increased by 8-, 5-, and 4-fold, respectively, between the two high-fat-fed groups of different ages. The sirtuin-mediated acetylation of the of urea cycle enzymes in aging tissue (70) and in response to caloric restriction (71) has been previously described for liver, but not for adipose tissue. Future studies are needed to understand the role and the regulation of arginine and methionine metabolism in adipose tissue maturation in response to caloric shifts.

In response to short term high fat feeding, we found prominent perturbations of lipid, carbohydrate, and mitochondria metabolism pathways, but did not capture significant changes in proteins associated with inflammatory or immune response changes. Current consensus is that inflammatory alterations in white adipose tissue underlie complications of obesity including diabetes mellitus (72, 73). High fat feeding leads to the recruitment of proinflammatory macrophages in adipose tissue and a switch from an anti-inflammatory milieu to a more proinflammatory milieu (74, 75). Proinflammatory cytokines such as TNFα and IL1-β have been implicated in the link between adipose tissue inflammation and insulin resistance (76, 77). In our experimental setting, even though the glucose homeostasis and insulin sensitivity declined as early as week 8 of high fat feeding, proteome changes in inflammatory pathways were only captured with long term high fat diet. Following 8 weeks of high fat feeding, despite increased body weight, development of glucose intolerance and decrease in insulin sensitivity, we did not capture changes at gene expression level for common inflammatory markers such as IL-1β, TNFα, IL-6, (only IL12α was modestly decreased) in the SVF suggesting no alterations in inflammatory status. This is consistent with reports where adipose tissue inflammation does not match the insulin sensitivity status (19, 78, 79). During the last 20 years, large numbers of studies in rodents and humans have suggested a mechanistic link between inflammatory response and a decline in metabolic state (50). Others have demonstrated a disconnect between adiposity, immune response and insulin resistance (78, 79). However, immune based therapeutic strategies to treat metabolic diseases have not emerged. Further studies are required to understand the extent and the nature of the immune pathways involved in adipose tissue in response to high fat feeding and aging. Our data suggests that other, less investigated pathways, such as extracellular remodeling, branch chain amino acid, and urea cycle should be integrated into our understanding of the adipose tissue metabolism and the implications on peripheral insulin resistance.

Our data is in concordance with the recent report from Serrano *et al.* showing that extracellular matrix proteins such as metalloproteinases, laminin and collagenase are decreased in aged adipose tissue. We observe the same effect in the aging mice fed high fat diet. It is interesting that they observe increased levels of inflammatory proteins only in gender comparison in men *versus* women, but not in nondiabetic *versus* diabetic comparison. We show a decrease in complement activation inflammatory proteins with increased high fat diet exposure.

For the short-term high fat diet group, our network analysis revealed the BCAA genes as key driver genes, supporting a central role of BCAA metabolism in the dysregulation of lipid, carbohydrate, and mitochondria metabolic processes. BCAA metabolism is proposed to play a role in obesity driven insulin resistance (64). Short term high fat fed mice are glucose intolerant and display mild insulin insensitivity. It has been proposed that adipose tissue inflammation in response to high fat feeding leads to insulin resistance via release of free fatty acids that activate the immune system and lead to release of cytokines (74, 80). We did not detect perturbation of the immune system by either gene enrichment analysis or key driver network analysis in short term high fat feeding. In our study, the activation of the immune system required longer high fat feeding and or maturation of the adipose tissue along with high fat diet. It is possible that perturbation of BCCA metabolism precedes the well-described adipose tissue inflammatory response commonly associated with obesity-driven insulin resistance. Investigation of the role of BCAA perturbation in insulin resistance and immune alteration is warranted. Our studies are limited to network analyses from curated databases for gene-gene interaction and lack metabolic validation. Future studies examining the interaction of prolonged aging and western diet are needed to elucidate the pathogenesis of metabolic diseases over a lifetime.

In contrast to the two groups discussed above, the high fat diet aging signature and the long-term high fat feeding signatures share large numbers of putative key driver genes such as F2, Serping1, and Alox5ap, and bear similar gene subnetwork structures. Interestingly, these three putative key driver

genes were identified as protein signatures in response to the effect of age on bovine subcutaneous fat proteome (81), suggesting the conserved roles of the predicted key driver subnetworks in adipose tissue. These genes are primarily involved in inflammation, complement and coagulation processes, suggesting that long-term high fat feeding produces a dominating inflammatory response through these potential regulators. Future studies are required to describe the roles of putative key driver genes F2, Serping1, and Alox5ap in adipose tissue metabolism.

Profiling the adipose tissue proteomic signatures in response to low and high fat diet identified pathways that were not available through gene expression studies. Microarray profiling based studies identify differentially expressed genes involved in immune response, extracellular matrix, lipid and carbohydrate metabolism (3, 82, 83) for comparable metabolic shifts. The urea cycle, renin angiotensin system, branch chain amino acid, and the methionine metabolism pathways were only revealed through proteomic profiling. Our findings are descriptive; however, they offer fertile grounds for future studies for validation and assessment of metabolic effect size. Describing the protein signatures are the first steps toward our understanding of the tissue's biological response to metabolic changes and will be followed by mechanistic studies.

In summary, we developed a novel proteome profiling approach and applied it to study adipose biology in response to metabolic perturbation and aging. By layering genetic and proteomic networks with metabolic profiles, we identified numerous protein signatures that translated to biological pathways, and gene networks that may underlie metabolic alterations. Three major patterns emerged: up-regulation of urea cycle in age related responses, down-regulation of complement activation for high fat diet changes, and up-regulation of branch chain amino acid metabolism in high fat diet related changes. We highlighted the relationships between genes and gene products in response to high-fat diet and advancing age, and pinpointed novel key regulators for these processes to facilitate future mechanistic studies.

* This work was supported by American Heart Association 3SDG16940064 (to N. Pamir), NIH core grants P30EY010572 & P30CA069533, and shared instrument grant S10OD012246. (to L. David), NIH/NIDDK R01DK104363, American Heart Association 13SDG17290032, and the Leducq Foundation Transatlantic Networks of Excellence Grant (to X. Yang), and American Heart Association 16POST31160044 (to Y. Zhao). The content is solely the responsibility of the authors and does not necessarily represent the official views of the National Institutes of Health.

S This article contains supplemental material.

‖ To whom correspondence should be addressed: Knight Cardiovascular Institute, Department of Medicine, OHSU, 3181 SW Sam Jackson Park Road, Portland, OR, 97239, Tel.: 503-346-1568; E-mail: pamir@ohsu.edu.

REFERENCES

1. Rosen, E. D., and MacDougald, O. A. (2006) Adipocyte differentiation from the inside out. *Nat. Rev. Mol. Cell Biol.* **7,** 885–896
2. Kim, H.-S., Ryoo, Z. Y., Choi, S. U., and Lee, S. (2015) Gene expression profiles reveal effect of a high-fat diet on the development of white and brown adipose tissues. *Gene* **565,** 15–21
3. Morita, S., Nakabayashi, K., Kawai, T., Hayashi, K., Horii, T., Kimura, M., Kamei, Y., Ogawa, Y., Hata, K., and Hatada, I. (2016) Gene expression profiling of white adipose tissue reveals paternal transmission of proneness to obesity. *Nature Publishing Group* **6,** 21693
4. Meierhofer, D., Weidner, C., and Sauer, S. (2014) Integrative analysis of transcriptomics, proteomics, and metabolomics data of white adipose and liver tissue of high-fat diet and rosiglitazone-treated insulin-resistant mice identified pathway alterations and molecular hubs. *J. Proteome Res.* **13,** 5592–5602
5. Forner, F., Kumar, C., Luber, C. A., Fromme, T., Klingenspor, M., and Mann, M. (2009) Proteome differences between brown and white fat mitochondria reveal specialized metabolic functions. *Cell Metabolism* **10,** 324–335
6. Kim, M.-S., Pinto, S. M., Getnet, D., Nirujogi, R. S., Manda, S. S., Chaerkady, R., Madugundu, A. K., Kelkar, D. S., Isserlin, R., Jain, S., Thomas, J. K., Muthusamy, B., Leal-Rojas, P., Kumar, P., Sahasrabuddhe, N. A., Balakrishnan, L., Advani, J., George, B., Renuse, S., Selvan, L. D. N., Patil, A. H., Nanjappa, V., Radhakrishnan, A., Prasad, S., Subbannayya, T., Raju, R., Kumar, M., Sreenivasamurthy, S. K., Marimuthu, A., Sathe, G. J., Chavan, S., Datta, K. K., Subbannayya, Y., Sahu, A., Yelamanchi, S. D., Jayaram, S., Rajagopalan, P., Sharma, J., Murthy, K. R., Syed, N., Goel, R., Khan, A. A., Ahmad, S., Dey, G., Mudgal, K., Chatterjee, A., Huang, T.-C., Zhong, J., Wu, X., Shaw, P. G., Freed, D., Zahari, M. S., Mukherjee, K. K., Shankar, S., Mahadevan, A., Lam, H., Mitchell, C. J., Shankar, S. K., Satishchandra, P., Schroeder, J. T., Sirdeshmukh, R., Maitra, A., Leach, S. D., Drake, C. G., Halushka, M. K., Prasad, T. S. K., Hruban, R. H., Kerr, C. L., Bader, G. D., Iacobuzio-Donahue, C. A., Gowda, H., and Pandey, A. (2014) A draft map of the human proteome. *Nature* **509,** 575–581
7. Wilhelm, M., Schlegl, J., Hahne, H., Moghaddas Gholami, A., Lieberenz, M., Savitski, M. M., Ziegler, E., Butzmann, L., Gessulat, S., Marx, H., Mathieson, T., Lemeer, S., Schnatbaum, K., Reimer, U., Wenschuh, H., Mollenhauer, M., Slotta-Huspenina, J., Boese, J.-H., Bantscheff, M., Gerstmair, A., Faerber, F., and Kuster, B. (2014) Mass-spectrometry-based draft of the human proteome. *Nature* **509,** 582–587
8. Meierhofer, D., Hartmann, L., and Sauer, S. (2013) Protein sets define disease states and predict in vivo effects of drug treatment. *Mol. Cell. Proteomics* **12,** 1965–1979
9. Joo, J. I., Oh, T. S., Kim, D. H., Choi, D. K., Wang, X., Choi, J.-W., and Yun, J. W. (2011) Differential expression of adipose tissue proteins between obesity-susceptible and -resistant rats fed a high-fat diet. *Proteomics* **11,** 1429–1448
10. Okita, N., Hayashida, Y., Kojima, Y., Fukushima, M., Yuguchi, K., Mikami, K., Yamauchi, A., Watanabe, K., Noguchi, M., Nakamura, M., Toda, T., and Higami, Y. (2012) Differential responses of white adipose tissue and brown adipose tissue to caloric restriction in rats. *Mech. Ageing Develop.* **133,** 255–266
11. Gómez-Serrano, M., Camafeita, E., García-Santos, E., López, J. A., Rubio, M. A., Sánchez-Pernaute, A., Torres, A., Vázquez, J., and Peral, B. (2016) Proteome-wide alterations on adipose tissue from obese patients as age-, diabetes- and gender-specific hallmarks. *Nature Publishing Group* **6,** 25756
12. Zhang, S.-D., and Gant, T. W. (2005) Effect of pooling samples on the efficiency of comparative studies using microarrays. *Bioinformatics* **21,** 4378–4383
13. Okita, N., Hayashida, Y., Kojima, Y., Fukushima, M., Yuguchi, K., Mikami, K., Yamauchi, A., Watanabe, K., Noguchi, M., Nakamura, M., Toda, T., and Higami, Y. (2012) Differential responses of white adipose tissue and brown adipose tissue to caloric restriction in rats. *Mech. Ageing Develop.* **133,** 255–266
14. Vogel, C., and Marcotte, E. M. (2012) Insights into the regulation of protein abundance from proteomic and transcriptomic analyses. *Nat. Rev. Genet.* **13,** 227–232
15. Gry, M., Rimini, R., Strömberg, S., Asplund, A., Pontén, F., Uhlen, M., and Nilsson, P. (2009) Correlations between RNA and protein expression profiles in 23 human cell lines. *BMC Genomics* **10,** 365
16. Ghazalpour, A., Bennett, B., Petyuk, V. A., Orozco, L., Hagopian, R., Mungrue, I. N., Farber, C. R., Sinsheimer, J., Kang, H. M., Furlotte, N., Park, C. C., Wen, P.-Z., heather, B., karl W., david, C. G. Pan, C., Yordanova,

R., Neuhaus, I., charles, T., nathan S., peter G., eleazar E., Kirchgessner, T., desmond, S. J., Richard, S. D., and aldon, L. J. (2011) Comparative analysis of proteome and transcriptome variation in mouse. *PLoS Genet.* **7,** e1001393
17. Thompson, A., Schäfer, J., Kuhn, K., Kienle, S., Schwarz, J., Schmidt, G., Neumann, T., Johnstone, R., Mohammed, A. K. A., and Hamon, C. (2003) Tandem mass tags: a novel quantification strategy for comparative analysis of complex protein mixtures by MS/MS. *Anal. Chem.* **75,** 1895–1904
18. Pamir, N., McMillen, T. S., Edgel, K. A., Kim, F., and LeBoeuf, R. C. (2012) Deficiency of lymphotoxin-α does not exacerbate high-fat diet-induced obesity but does enhance inflammation in mice. **302,** E961–E971
19. Pamir, N., McMillen, T. S., Kaiyala, K. J., Schwartz, M. W., and LeBoeuf, R. C. (2009) Receptors for tumor necrosis factor-alpha play a protective role against obesity and alter adipose tissue macrophage status. *Endocrinology* **150,** 4124–4134
20. Pamir, N., Liu, N.-C., Irwin, A., Becker, L., Peng, Y., Ronsein, G. E., Bornfeldt, K. E., Duffield, J. S., and Heinecke, J. W. (2015) Granulocyte/macrophage colony-stimulating factor-dependent dendritic cells restrain lean adipose tissue expansion. *J. Biol. Chem.* **290,** 14656–14667
21. Soukas, A., Socci, N. D., Saatkamp, B. D., Novelli, S., and Friedman, J. M. (2001) Distinct transcriptional profiles of adipogenesis in vivo and in vitro. *J. Biol. Chem.* **276,** 34167–34174
22. Livak, K. J., and Schmittgen, T. D. (2001) Analysis of relative gene expression data using real-time quantitative PCR and the 2(-Delta Delta C(T)) Method. *Methods* **25,** 402–408
23. Senko, M. W., Remes, P. M., Canterbury, J. D., Mathur, R., Song, Q., Eliuk, S. M., Mullen, C., Earley, L., Hardman, M., Blethrow, J. D., Bui, H., Specht, A., Lange, O., Denisov, E., Makarov, A., Horning, S., and Zabrouskov, V. (2013) Novel Parallelized Quadrupole/Linear Ion Trap/Orbitrap Tribrid Mass Spectrometer Improving Proteome Coverage and Peptide Identification Rates. *Anal. Chem.* **85,** 11710–11714
24. Hsieh, E. J., Hoopmann, M. R., MacLean, B., and MacCoss, M. J. (2010) Comparison of database search strategies for high precursor mass accuracy MS/MS data. *J. Proteome Res.* **9,** 1138–1143
25. Käll, L., Canterbury, J. D., Weston, J., Noble, W. S., and MacCoss, M. J. (2007) Semi-supervised learning for peptide identification from shotgun proteomics datasets. *Nat. Methods* **4,** 923–925
26. Robinson, M. D., McCarthy, D. J., and Smyth, G. K. (2010) edgeR: a Bioconductor package for differential expression analysis of digital gene expression data. *Bioinformatics* **26,** 139–140
27. Zhu, J., Bin Zhang Smith, E. N., Drees, B., Brem, R. B., Kruglyak, L., Bumgarner, R. E., and Schadt, E. E. (2008) Integrating large-scale functional genomic data to dissect the complexity of yeast regulatory networks. *Nat. Genet.* **40,** 854–861
28. Zhu, J., Wiener, M. C., Zhang, C., Fridman, A., Minch, E., Lum, P. Y., Sachs, J. R., and Schadt, E. E. (2007) Increasing the Power to Detect Causal Associations by Combining Genotypic and Expression Data in Segregating Populations. *PLoS Comput. Biol.* **3,** e69
29. Wang, I.-M., Bin Zhang Yang, X., Zhu, J., Stepaniants, S., Zhang, C., Meng, Q., Peters, M., He, Y., Ni, C., Slipetz, D., Crackower, M. A., Houshyar, H., Tan, C. M., Appiah, E. A., O'Neill, G., Luo, M. J., Thieringer, R., Yuan, J., Chiu, C. S., Lum, P. Y., Lamb, J., Boie, Y., Wilkinson, H. A., Schadt, E. E., Dai, H., and Roberts, C. (2012) Systems analysis of eleven rodent disease models reveals an inflammatome signature and key drivers. *Mol. Syst. Biol.* **8,** 594–594
30. Yang, X., Zhang, B., Molony, C., Chudin, E., Hao, K., Zhu, J., Gaedigk, A., Suver, C., Zhong, H., Leeder, J. S., Guengerich, F. P., Strom, S. C., Schuetz, E., Rushmore, T. H., Ulrich, R. G., Slatter, J. G., Schadt, E. E., Kasarskis, A., and Lum, P. Y. (2010) Systematic genetic and genomic analysis of cytochrome P450 enzyme activities in human liver. *Genome Res.* **20,** 1020–1036
31. Mäkinen, V.-P., Civelek, M., Meng, Q., Zhang, B., Zhu, J., Levian, C., Huan, T., Segrè, A. V., Ghosh, S., Vivar, J., Nikpay, M., Stewart, A. F. R., Nelson, C. P., Willenborg, C., Erdmann, J., Blakenberg, S., O'Donnell, C. J., Marz, W., Laaksonen, R., Epstein, S. E., Kathiresan, S., Shah, S. H., Hazen, S. L., Reilly, M. P., Coronary ARtery DIsease Genome-Wide Replication And Meta-Analysis (CARDIoGRAM) Consortium Lusis, A. J., Samani, N. J., Schunkert, H., Quertermous, T., McPherson, R., Yang, X., and Assimes, T. L. (2014) Integrative genomics reveals novel molecular pathways and gene networks for coronary artery disease. *PLoS Genet.* **10,** e1004502
32. Benjamini, Y., and Hochberg, Y. (1995) Controlling the false discovery rate: a practical and powerful approach to multiple testing. *J. Roy. Statistical Soc.* **57,** 289–300
33. Vizcaíno, J. A., Csordas, A., del-Toro, N., Dianes, J. A., Griss, J., Lavidas, I., Mayer, G., Perez-Riverol, Y., Reisinger, F., Ternent, T., Xu, Q.-W., Wang, R., and Hermjakob, H. (2016) 2016 update of the PRIDE database and its related tools. *Nucleic Acids Res.* **44,** D447–D56
34. Wenger, C. D., Phanstiel, D. H., Lee, M. V., Bailey, D. J., and Coon, J. J. (2011) COMPASS: A suite of pre- and post-search proteomics software tools for OMSSA. *Proteomics* **11,** 1064–1074
35. McCarthy, D. J., Chen, Y., and Smyth, G. K. (2012) Differential expression analysis of multifactor RNA-Seq experiments with respect to biological variation. *Nucleic Acids Res.* **40,** 4288–4297
36. Fei, S. S., Wilmarth, P. A., Hitzemann, R. J., McWeeney, S. K., Belknap, J. K., and David, L. L. (2011) Protein database and quantitative analysis considerations when integrating genetics and proteomics to compare mouse strains. *J. Proteome Res.* **10,** 2905–2912
37. Branson, O. E., and Freitas, M. A. (2016) A multi-model statistical approach for proteomic spectral count quantitation. *J. Proteomics* **144,** 23–32
38. Huan, J., Hornick, N. I., Goloviznina, N. A., Kamimae- Lanning, A. N., David, L. L., Wilmarth, P. A., Mori, T., Chevillet, J. R., Narla, A., Roberts, C. T., Loriaux, M. M., Chang, B. H., and Kurre, P. (2015) Coordinate regulation of residual bone marrow function by paracrine trafficking of AML exosomes. *Leukemia* **29,** 2285–2295
39. Midgett, M., López, C. S., David, L., Maloyan, A., and Rugonyi, S. (2017) Increased hemodynamic load in early embryonic stages alters endocardial to mesenchymal transition. *Front. Physiol.* **8,** 56
40. Anders, S., McCarthy, D. J., Chen, Y., Okoniewski, M., Smyth, G. K., Huber, W., and Robinson, M. D. (2013) Count-based differential expression analysis of RNA sequencing data using R and Bioconductor. *Nat. Protocols* **8,** 1765–1786
41. Huang, D. W., Sherman, B. T., and Lempicki, R. A. (2009) Systematic and integrative analysis of large gene lists using DAVID bioinformatics resources. *Nat. Protocols* **4,** 44–57
42. Lin, Y., Berg, A. H., Iyengar, P., Lam, T. K. T., Giacca, A., Combs, T. P., Rajala, M. W., Du, X., Rollman, B., Li, W., Hawkins, M., Barzilai, N., Rhodes, C. J., Fantus, I. G., Brownlee, M., and Scherer, P. E. (2005) The hyperglycemia-induced inflammatory response in adipocytes: the role of reactive oxygen species. *J. Biol. Chem.* **280,** 4617–4626
43. Van Ziffle, J. A., and Lowell, C. A. (2009) Neutrophil-specific deletion of Syk kinase results in reduced host defense to bacterial infection. *Blood* **114,** 4871–4882
44. Mócsai, A., Abram, C. L., Jakus, Z., Hu, Y., Lanier, L. L., and Lowell, C. A. (2006) Integrin signaling in neutrophils and macrophages uses adaptors containing immunoreceptor tyrosine-based activation motifs. *Nat. Immunol.* **7,** 1326–1333
45. Soronen, J., Laurila, P.-P., Naukkarinen, J., Surakka, I., Ripatti, S., Jauhiainen, M., Olkkonen, V. M., and Yki-Järvinen, H. (2012) Adipose tissue gene expression analysis reveals changes in inflammatory, mitochondrial respiratory and lipid metabolic pathways in obese insulin-resistant subjects. *BMC Med. Gen. 2012 5:1* **5,** 9
46. Osma-García, I. C., Cacheiro-Llaguno, C., Fresno, M., diaz-munoz. (2010) Coordinated up-regulation of cyclooxygenase-2 and microsomal prostaglandin E synthase 1 transcription by nuclear factor kappa B and early growth response-1 in macrophages. *Cell. Signal.* **22,** 1427–1436
47. Kanter, J. E., Kramer, F., Barnhart, S., Averill, M. M., Vivekanandan-Giri, A., Vickery, T., Li, L. O., Becker, L., Yuan, W., Chait, A., Braun, K. R., Potter-Perigo, S., Sanda, S., Wight, T. N., Pennathur, S., Serhan, C. N., Heinecke, J. W., Coleman, R. A., and Bornfeldt, K. E. (2012) Diabetes promotes an inflammatory macrophage phenotype and atherosclerosis through acyl-CoA synthetase 1. *Proc. Natl. Acad. Sci. U S A* **109,** E715–E24
48. Takahashi, N., Li, F., Hua, K., Deng, J., Wang, C.-H., Bowers, R. R., Bartness, T. J., Kim, H.-S., and Harp, J. B. (2007) Increased energy expenditure, dietary fat wasting, and resistance to diet-induced obesity in mice lacking renin. *Cell Metab.* **6,** 506–512
49. Jayasooriya, A. P., Mathai, M. L., Walker, L. L., Begg, D. P., Denton, D. A., Cameron-Smith, D., Egan, G. F., McKinley, M. J., Rodger, P. D., Sinclair, A. J., Wark, J. D., Weisinger, H. S., Jois, M., and Weisinger, R. S. (2008) Mice lacking angiotensin-converting enzyme have increased energy ex-

penditure, with reduced fat mass and improved glucose clearance. *Proc. Natl. Acad. Sci. U S A* **105,** 6531–6536
50. Olefsky, J. M., and Glass, C. K. (2010) Macrophages, inflammation, and insulin resistance. *Annu. Rev. Physiol.* **72,** 219–246
51. Santer, R., Rischewski, J., Weihe, von, M., Niederhaus, M., Schneppenheim, S., Baerlocher, K., Kohlschütter, A., Muntau, A., Posselt, H.-G., Steinmann, B., and Schneppenheim, R. (2005) The spectrum of aldolase B (ALDOB) mutations and the prevalence of hereditary fructose intolerance in Central Europe. *Hum. Mutat.* **25,** 594
52. Mutch, D. M., Pers, T. H., Temanni, M. R., Pelloux, V., Marquez-Quiñones, A., Holst, C., Martinez, J. A., Babalis, D., van Baak, M. A., Handjieva-Darlenska, T., Walker, C. G., Astrup, A., Saris, W. H. M., Langin, D., Viguerie, N., Zucker, J.-D., Clément, K., DiOGenes Project. (2011) A distinct adipose tissue gene expression response to caloric restriction predicts 6-mo weight maintenance in obese subjects. *Am. J. Clin. Nutr.* **94,** 1399–1409
53. Teng, Y.-W., Ellis, J. M., Coleman, R. A., and Zeisel, S. H. (2012) Mouse betaine-homocysteine S-methyltransferase deficiency reduces body fat via increasing energy expenditure and impairing lipid synthesis and enhancing glucose oxidation in white adipose tissue. *Journal of Biol. Chem.* **287,** 16187–16198
54. Lumeng, C. N., Bodzin, J. L., and Saltiel, A. R. (2007) Obesity induces a phenotypic switch in adipose tissue macrophage polarization. *J. Clin. Invest.* **117,** 175–184
55. Gabrilovich, D. I., and Nagaraj, S. (2009) Myeloid-derived suppressor cells as regulators of the immune system. *Nat. Rev. Immunol.* **9,** 162–174
56. Wu, D., Ren, Z., Pae, M., Guo, W., Cui, X., Merrill, A. H., and Meydani, S. N. (2007) Aging Up-Regulates Expression of Inflammatory Mediators in Mouse Adipose Tissue. *J. Immunol.* **179,** 4829–4839
57. López-Otín, C., Blasco, M. A., Partridge, L., Serrano, M., and Kroemer, G. (2013) The hallmarks of aging. *Cell* **153,** 1194–1217
58. Derry, J. M. J., Zhong, H., Molony, C., MacNeil, D., GuhaThakurta, D., Bin Zhang Mudgett, J., Small, K., Fertak El, L., Guimond, A., Selloum, M., Zhao, W., Champy, M.-F., Monassier, L., Vogt, T., Cully, D., Kasarskis, A., and Schadt, E. E. (2010) Identification of genes and networks driving cardiovascular and metabolic phenotypes in a mouse F2 intercross. *PLoS ONE* **5,** e14319
59. Emilsson, V., Thorleifsson, G., Zhang, B., Leonardson, A. S., Zink, F., Zhu, J., Carlson, S., Helgason, A., Walters, G. B., Gunnarsdottir, S., Mouy, M., Steinthorsdottir, V., Eiriksdottir, G. H., Bjornsdottir, G., Reynisdottir, I., Gudbjartsson, D., Helgadottir, A., Jonasdottir, A., Jonasdottir, A., Styrkarsdottir, U., Gretarsdottir, S., Magnusson, K. P., Stefansson, H., Fossdal, R., Kristjansson, K., Gislason, H. G., Stefansson, T., Leifsson, B. G., Thorsteinsdottir, U., Lamb, J. R., Gulcher, J. R., Reitman, M. L., Kong, A., Schadt, E. E., and Stefansson, K. (2008) Genetics of gene expression and its effect on disease. *Nature* **452,** 423–428
60. Greenawalt, D. M., Dobrin, R., Chudin, E., Hatoum, I. J., Suver, C., Beaulaurier, J., Zhang, B., Castro, V., Zhu, J., Sieberts, S. K., Wang, S., Molony, C., Heymsfield, S. B., Kemp, D. M., Reitman, M. L., Lum, P. Y., Schadt, E. E., and Kaplan, L. M. (2011) A survey of the genetics of stomach, liver, and adipose gene expression from a morbidly obese cohort. *Genome Res.* **21,** 1008–1016
61. Yang, X., Schadt, E. E., Wang, S., Wang, H., Arnold, A. P., Ingram-Drake, L., Drake, T. A., and Lusis, A. J. (2006) Tissue-specific expression and regulation of sexually dimorphic genes in mice. *Genome Res.* **16,** 995–1004
62. Chen, Y., Zhu, J., Lum, P. Y., Yang, X., Pinto, S., MacNeil, D. J., Zhang, C., Lamb, J., Edwards, S., Sieberts, S. K., Leonardson, A., Castellini, L. W., Wang, S., Champy, M.-F., Zhang, B., Emilsson, V., Doss, S., Ghazalpour, A., Horvath, S., Drake, T. A., Lusis, A. J., and Schadt, E. E. (2008) Variations in DNA elucidate molecular networks that cause disease. *Nature* **452,** 429–435
63. Pietiläinen, K. H., Naukkarinen, J., Rissanen, A., Saharinen, J., Ellonen, P., Keränen, H., Suomalainen, A., Götz, A., Suortti, T., Yki-Järvinen, H., Oresic, M., Kaprio, J., and Peltonen, L. (2008) Global transcript profiles of fat in monozygotic twins discordant for BMI: pathways behind acquired obesity. *PLoS Med.* **5,** e51
64. Newgard, C. B., An, J., Bain, J. R., Muehlbauer, M. J., Stevens, R. D., Lien, L. F., Haqq, A. M., Shah, S. H., Arlotto, M., Slentz, C. A., Rochon, J., Gallup, D., Ilkayeva, O., Wenner, B. R., Yancy, W. S., Eisenson, H., Musante, G., Surwit, R. S., Millington, D. S., Butler, M. D., and Svetkey, L. P. (2009) A branched-chain amino acid-related metabolic signature that differentiates obese and lean humans and contributes to insulin resistance. *Cell Metabolism* **9,** 311–326
65. Després, J.-P. (2012) Body fat distribution and risk of cardiovascular disease: an update. *Circulation* **126,** 1301–1313
66. Lumeng, C. N., and Saltiel, A. R. (2011) Inflammatory links between obesity and metabolic disease. *J. Clin. Invest.* **121,** 2111–2117
67. Després, J.-P., and Lemieux, I. (2006) Abdominal obesity and metabolic syndrome. *Nature* **444,** 881–887
68. Guyenet, S. J., and Schwartz, M. W. (2012) Clinical review: Regulation of food intake, energy balance, and body fat mass: implications for the pathogenesis and treatment of obesity. *J. Clin. Endocrinol. Metab.* **97,** 745–755
69. Morris, S. M. (2002) Regulation of enzymes of the urea cycle and arginine metabolism. *Annu. Rev. Nutr.* **22,** 87–105
70. Nakagawa, T., Lomb, D. J., Haigis, M. C., and Guarente, L. (2009) SIRT5 Deacetylates carbamoyl phosphate synthetase 1 and regulates the urea cycle. *Cell* **137,** 560–570
71. Hallows, W. C., Yu, W., Smith, B. C., Devries, M. K., Devires, M. K., Ellinger, J. J., Someya, S., Shortreed, M. R., Prolla, T., Markley, J. L., Smith, L. M., Zhao, S., Guan, K.-L., and Denu, J. M. (2011) Sirt3 promotes the urea cycle and fatty acid oxidation during dietary restriction. *Mol. Cell* **41,** 139–149
72. Hotamisligil, G. S. (2006) Inflammation and metabolic disorders. *Nature* **444,** 860–867
73. Donath, M. Y., and Shoelson, S. E. (2011) Type 2 diabetes as an inflammatory disease. *Nat. Rev. Immunol.* **11,** 98–107
74. Chawla, A., Nguyen, K. D., and Goh, Y. P. S. (2011) Macrophage-mediated inflammation in metabolic disease. *Nat. Rev. Immunol.* **11,** 738–749
75. Lumeng, C. N., Bodzin, J. L., and Saltiel, A. R. (2007) Obesity induces a phenotypic switch in adipose tissue macrophage polarization. *J. Clin. Invest.* **117,** 175–184
76. Hotamisligil, G. S., Shargill, N. S., and Spiegelman, B. M. (1993) Adipose expression of tumor necrosis factor-alpha: direct role in obesity-linked insulin resistance. *Science* **259,** 87–91
77. Lumeng, C. N., and Saltiel, A. R. (2011) Inflammatory links between obesity and metabolic disease. *J. Clin. Invest.* **121,** 2111–2117
78. Pamir, N., McMillen, T. S., Edgel, K. A., Kim, F., and LeBoeuf, R. C. (2012) Deficiency of lymphotoxin-α does not exacerbate high-fat diet-induced obesity but does enhance inflammation in mice. *AJP: Endocrinol. Metabolism* **302,** E961–E71
79. Lee, J.-T., Pamir, N., Liu, N.-C., Kirk, E. A., Averill, M. M., Becker, L., Larson, I., Hagman, D. K., Foster-Schubert, K. E., van Yserloo, B., Bornfeldt, K. E., LeBoeuf, R. C., Kratz, M., and Heinecke, J. W. (2014) Macrophage metalloelastase (MMP12) regulates adipose tissue expansion, insulin sensitivity, and expression of inducible nitric oxide synthase. *Endocrinology* **155,** 3409–3420
80. Ferrante, A. W. (2013) Macrophages, fat, and the emergence of immunometabolism. *J. Clin. Invest.* **123,** 4992–4993
81. Romao, J. M., He, M. L., McAllister, T. A., and Guan, L. L. (2014) Effect of age on bovine subcutaneous fat proteome: Molecular mechanisms of physiological variations during beef cattle growth. *J. Animal Sci.* **92,** 3316–3327
82. Voigt, A., Agnew, K., Schothorst, E. M., Keijer, J., and Klaus, S. (2013) Short-term, high fat feeding-induced changes in white adipose tissue gene expression are highly predictive for long-term changes. *Mol. Nutrition Food Res.* **57,** 1423–1434
83. Kwon, E.-Y., Shin, S.-K., Cho, Y.-Y., Jung, U. J., Kim, E., Park, T., Park, J. H. Y., Yun, J. W., McGregor, R. A., Park, Y. B., and Choi, M.-S. (2012) Time-course microarrays reveal early activation of the immune transcriptome and adipokine dysregulation leads to fibrosis in visceral adipose depots during diet-induced obesity. *BMC Genomics* **13,** 450